Quantum interference effects for strongly localized electrons

Ernesto Medina
Coordinación de Investigación Básica, Intevep SA, Apartado 76343, Caracas 1070A, Venezuela

Mehran Kardar
Department of Physics, Massachusetts Institute of Technology, Cambridge, Massachusetts 02139
(Received 8 November 1991)

We examine the role of quantum interference phenomena for strongly localized electrons. The probability distribution for tunneling between two sites separated at a distance t is computed numerically and analytically by summing all *forward scattering paths*. We find a *universal* probability distribution that is approximately log normal; its mean proportional to t, its variance growing as $t^{2\omega}$, with ω depending on the dimension d. Since the mean and variance of the distribution are independent, *two parameters* are necessary to describe the tunneling probability. High moments of the distribution are, however, nonuniversal, and dominated by exceptionally good samples. We also study the response of the system to a magnetic field B, with and without spin-orbit (SO) scattering. Without SO a magnetic field leads to a small (nonuniversal) increase in the localization length ξ scaling as $B^{1/2}$. With SO there is still a positive magnetoconductance (initially scaling as B^2t^3, although there is no change in the localization length). The above results, obtained from extensive numerical simulations, can be analytically explained by a replica analysis of moments. They follow from properties of a bound state between replicas: the attraction factor is related to the symmetries of the underlying Hamiltonian. Our results are compared and contrasted with current literature of the subject of strong localization.

I. INTRODUCTION AND SUMMARY

The past decade has witnessed great advances in the understanding of quantum-mechanical effects on electron transport in disordered systems. For noninteracting electrons, disorder causes a metal-insulator transition by localizing the electronic states.[1] The original ideas of Anderson localization,[1] and a heuristic scaling approach by Thouless,[2] were placed on a more rigorous footing by perturbative renormalization-group studies.[3-5] In addition to providing a systematic basis for the study of the localization transition in $d=2+\varepsilon$ dimensions, the perturbative approach also describes the role of quantum interference effects in the weakly disordered metal. Such *weak-localization* phenomena include the effects of magnetic fields, spin-orbit scattering (SO) (corresponding, respectively, to perturbations breaking time-reversal and spin space symmetries) on the conductivity,[6] and also the universal nature of conductance fluctuations.[7,8] In the absence SO, a magnetic field causes an increase in the localization length, and a factor-of-2 decrease in the conductance fluctuations; with SO, it has the opposite effect of decreasing the localization length, while still reducing the conductance fluctuations.[9,10] These phenomena can be traced to the quantum interference of time-reversed paths in *backscattering* loops, and their suppression by magnetic fields and SO.[11] An alternative description of these phenomena is based on the theory of random matrices,[12] where the only input is the symmetries of the underlying Hamiltonian, and their modification by a magnetic field. Mesoscopic devices at low temperature have provided many experimental verification of *weak-localization* theory,[11,13] and there are many excellent reviews on the subject.[6,11,14]

By contrast, there have been few studies of the behavior of conductivity and its fluctuations for *strongly localized* electrons. The theoretical perturbative approaches to weak localization break down and are not appropriate in this regime. On the experimental side, it is much more difficult to measure the variations in the much smaller conductivities of insulators. The main mechanism for conductivity in this regime is by thermally activated quantum tunneling between the localized sites. According to Mott's description of variable-range hopping (VRH),[15] at lower temperatures T, the electron tunnels a greater distance to find a localized site of closer energy. Balancing the probabilities for hopping and thermal activation, Mott concluded that in d dimensions the tunneling length scales with temperature as

$$t \approx \xi (T_0/T)^{1/(d+1)} , \tag{1.1}$$

where T_0 is a characteristic temperature, and ξ is the localization radius of impurities at the Fermi level. In this regime, the optimal hopping length is many times greater than the localization length ξ. The localized sites are then assumed to be connected by a classical random resistor network.[16] Since the individual resistors are taken from a very wide distribution, it is then argued[17] that the resistance of the whole sample is governed by the critical resistor that makes the network percolate. This leads to a dependence

$$\sigma(T)=\sigma_0 \exp[-(T_0/T)^{1/(d+1)}] , \tag{1.2}$$

for the conductivity. This behavior has been verified experimentally both in two and three dimensions.[18]

How does a magnetic field influence the conductivity in the VRH regime? The simplest picture is that a magnetic field causes the impurity orbitals to shrink, leading to a decrease in the tunneling probability, i.e., a *negative* magnetoconductance (MC).[18,19] However, recent measurements[20–23] find a *positive* MC in Si-inversion layers, GaAs, and In_2O_{3-x} films. Furthermore, the observed reproducible conductance fluctuations are quite suggestive of quantum interference (QI) effects.[24–26] Nguyen, Spivak, and Shklovskii (NSS) (Ref. 27) have proposed a model that accounts for QI of multiply scattered tunneling paths in the hopping probability: In between the phonon-assisted tunneling events, the electron preserves its phase memory. However, at low temperatures, it tunnels over very large distances according to Eq. (1.1), and encounters many impurities. The overall tunneling amplitude is then obtained from the sum over all trajectories between the initial and final sites. NSS emphasized that since the contribution of each trajectory is exponentially small in its length, the dominant contributions to the sum come from the shortest or *forward-scattering* paths. The traditional explanations of weak-localization phenomena that rely on the QI of *backscattering* paths are therefore inappropriate to this regime.

Indeed, the MC and fluctuations observed experimentally, though qualitatively similar to those of a disordered metal, have considerably larger magnitudes.[26] There are three relevant length scales in the problem that must be discussed in order to make comparisons with experiments: the lattice spacing a, the localization length ξ, and the hopping length t. In all the experimental systems that exhibit VRH, the localization length ξ is much larger that the lattice spacing ($\xi \sim 10a$ at least), due to the weak binding of the donated electron (or donated hole) to the impurity center. This fact allows for localization only over many lattice spacings, and renders the localization phenomena relatively independent of the nature of the dopants. In contrast, the ratio t/ξ is more variable, and is (as we will discuss later) crucial in identifying the appropriate regime of validity of the directed-path approach. We note that the condition for the NSS model to give reasonable predictions is that the hopping length be much larger than the localization radius. This condition seems to be realized in the systems studied experimentally: In_2O_{3-x} (Ref. 23) at temperatures in the mK range has $t \sim 5-10\xi$, while in the GaAs system $t \sim 5-6\xi$.[21] This is also true of the Y_xSi_{1-x} system in a recent study[28] where the condition $t \sim 8\xi$ can be reached for certain samples. When the hopping length becomes of the order of the localization length, the directed-path approximation is less appropriate, as backscattering becomes important and weak-localization effects set in. A scenario has been given by Zhao *et al.*[29] that illustrates the interplay between length scales: They suggest that one can divide the region of tunneling into blobs of the size of the localization length and assume that backscattering is important within each blob region, but not between blobs. When there are many blobs to a hopping length, paths connecting centers at the Fermi level are essentially directed and backscattering is therefore less important. On other hand, when the blob size is of the order of the upper cutoff given by the hopping length, the coherence region for VRH should be dominated by weak-localization mechanisms.

Numerical simulations of forward-scattering paths[27] in small systems indeed indicated a positive MC in qualitative agreement with the experiments. NSS also provided a theoretical explanation of their results by regarding the forward-scattering paths as independent random variables. This independent-path approach (IPA) was later combined with a percolation analysis of the random network,[30] and also extended to include SO effects.[31] Both in the presence and absence of SO, the IPA predicts a small positive MC ($\delta\sigma/\sigma \sim 1$), but no change in the localization length. The actual MC observed in experiments[26] is much larger. A different approach to the problem extends the random matrix approach (RMA) to strongly localized electrons.[32] The RMA predicts that a magnetic field leads to a doubling of the localization length ξ (big, positive MC) without SO, but a halving of ξ (big, negative MC) in the presence of SO. Yet a different heuristic argument[33] concludes that the factor-of-2 increase in ξ is only valid for quasi-one-dimensional systems, and predicts a nonuniversal increase in higher dimensions. Clearly, these approaches lead to conflicting predictions that we believe are due to inherent limitations of the approximations involved. Over the past three years we undertook extensive numerical studies of the NSS model. We used a transfer-matrix procedure that allowed exact summation of forward-scattering paths for very large systems ($t \approx 10^3-10^4$), and obtained statistics by averaging over many realizations ($\approx 10^3$) of randomness. These results, combined with some analytical insights, provide a coherent description of the behavior of strongly localized electrons. The main conclusions have already appeared in three short papers,[34–36] which give only sketches of the numerical simulations, and the essence of the theoretical arguments. The purpose of this paper is to provide the details, fill in the gaps, and also to report on a number of unreported new results.

To understand the general philosophy of this approach, it may be helpful to make a comparison to the problem of phase transitions in Heisenberg magnets.[37] The weak-localization approach is similar to the *low-temperature* expansion for magnets. One starts with the ordered phase (metal) and perturbatively includes fluctuations (randomness). Both approaches yield a (potentially exact) description of the correlations in the ordered phase, a perturbative $2+\varepsilon$ estimate of the exponents associated with the disordering transition, and are inapplicable to the disordered phase. To describe the correlation functions in the disordered phase of the magnet, *high-temperature* expansions have to be used. In such an expansion, the spin-spin-correlation function between two points is dominated by the shortest paths between them, and decays exponentially with their separation. This is qualitatively the same as the decay of localized wave functions, except that in the latter case there is an overall disorder that makes the correlation function inhomogeneous. Thus one should instead consider the whole probability distribution for the decay of the wave function. Indeed, different moments of the wave function

may well decay with different "localization lengths." The goal of this paper is to study this more complicated behavior of correlation functions in the disordered phase of a quenched random system. In the context of localization, the appropriate tool is the *locator* expansion,[1] which starts with completely localized sites, and perturbatively includes the wave-function overlaps. However, the structure of the series is similar to high-temperature expansions for spin glasses and random-bond magnets. We thus expect that the universal aspects of our results are equally applicable to the disordered phase of all of these systems. An outline of the conclusions is given below.

Section II introduces the NSS model, and explains the locator expansion[1] for the tunneling amplitude Ψ. The transfer-matrix procedure is then introduced as an efficient numerical algorithm to sum the contribution of forward-scattering paths to Ψ. The results from many realizations are then used to construct the probability distribution for tunneling $P(\Psi)$ as a function of the hopping range t. We find that the probability distribution is very broad, so that it is more appropriate to consider $P[\ln\Psi(t)]$. The average $\langle \ln\Psi(t)\rangle$ is proportional to t; its prefactor can thus be used to define an inverse localization length ξ^{-1}. The variance of $\ln\Psi(t)$ also grows with t, but only as $t^{2\omega}$ with $\omega=0.33\pm0.05$. An analytical interpretation of these results is provided by examining the moments $\langle \Psi(t)^n\rangle$ of the tunneling amplitude, which describes n interacting forward-scattering paths. The odd moments vanish by symmetry, while the even moments are dominated by n paired paths forming a bound state, implying

$$\langle \Psi(t)^n\rangle = \langle \Psi(t)\rangle^n \exp[\rho n(n^2-1)t] \ . \tag{1.3}$$

It follows from Eq. (1.3) that different moments have different decay lengths. Equation (1.3) is the characteristic function for $\ln\Psi$, and implies

$$\langle \ln\Psi(t)\rangle = \ln\langle \Psi(t)\rangle - \rho t \equiv -t/\xi \ . \tag{1.4}$$

The inverse localization length ξ^{-1} is thus the sum of a trivial part $\xi_0^{-1}=-\ln\langle \Psi(t)\rangle/t$, originating in local overlap and geometrical factors, and a global part $\xi_g^{-1}=\rho$ arising from the interference of all paths. From Eq. (1.3) we further deduce the scaling of fluctuations as

$$\delta \ln\Psi(t) \sim t^{1/3} \ , \tag{1.5}$$

in agreement with the numerical results. Section II concludes with some recent numerical results on the question of a possible *sign transition*[27] in two dimensions—we find no evidence for such a transition.

Section III examines the role of a magnetic field B on tunneling. We first examine the resulting intriguing interference patterns for tunneling under a regular lattice. This can be regarded as the extension of Hofstadter's work[38] to localized states. With disorder, our numerical results indicate that the form of the probability distribution in still the same as Eq. (1.3) but now the parameter ρ depends on the magnetic field B. Increasing B leads to an increase in the localization length (hence enhanced tunneling and a positive MC), and a sharpening of the distribution $P[\ln\Psi(t)]$. Both effects are consistent with a reduction in ρ, which in turn is theoretically explained in terms of the loosening of the bound state in replica space. The initial increase of the localization length is found to scale as $B^{1/2}$, i.e.,

$$\delta\langle \ln\Psi(t,B)\rangle \sim +B^{1/2}t \ . \tag{1.6}$$

The new results in this section describe the behavior of MC at very small magnetic fields, which may be more appropriate to the experiments.

The effects of spin-orbit scattering are studied in Sec. IV. As we are interested mostly in the universal properties, we examine the extreme limit of strong SO by randomly rotating the spin at each impurity site. Switching on the SO interactions leads to an immediate increase in the localization length ξ (reduction of ρ), but the addition of a magnetic field has no further effect on ξ. There is a much smaller enhancement of tunneling due to an increase in an overall prefactor to Eq. (1.3). Thus for both with and without SO, there is a positive MC, the latter is large and accompanied by an increase in ξ, while the former is small and there is no change in ξ. For small fields, the increase in MC, with SO, behaves as

$$\delta\langle \ln\Psi(t,B)\rangle_{\rm SO} \sim \begin{cases} B^2t^3 & \text{if } B^2t^3<1 \\ \text{const} & \text{if } B^2t^3>1 \ . \end{cases} \tag{1.7}$$

These results are clearly in conflict with the predictions of IPA and RMA reported earlier. We comment on the limitations of the approximations that lead to erroneous conclusions. An appealing picture emerges from examination of moments $\langle \Psi^{2n}(t,B)\rangle$ in replica space: The impurity averaging collapses the $2n$ paths into n pairs. Upon each intersection, the paired paths can exchange partners leading to an exchange attraction. The exchange factors reflect the symmetries of the Hamiltonian: 3 for orthogonal symmetry (no SO, $B=0$), 2 for unitary symmetry (no SO, large B), and $\frac{3}{2}$ for the symplectic case (with SO). The exchange attraction then binds the n pairs, and leads to the moments given in Eq. (1.3). The observed MC trends then reflect the changes in the exchange attraction upon including a magnetic field.

As mentioned earlier, Eq. (1.3) describes the behavior of moments of two-point correlation functions in the disordered phase of many *two-dimensional* systems: it is applicable to spin glasses, random-bond magnets, as well as localization. However, it cannot be valid for arbitrary large n, since it would imply an *increase* in correlations for sufficiently large n. This point is addressed in Sec. V, where we argue that the very high moments of the distribution are actually nonuniversal, and simply reflect the moments of local impurities. It is interesting that a similar nonuniversality is also observed close to the localization transition, in a weak-disorder expansion.[39] We provide both heuristic arguments and results on a hierarchical lattice that support this nonuniversality in the strongly disordered regime. All the results reported so far describe two-dimensional systems. Possible extensions and implications in higher dimensions conclude Sec. V.

If we accept the standard expressions for Mott variable-range hopping in Eqs. (1.1) and (1.2), then Eqs. (1.5)–(1.7) make quantitative predictions for the varia-

tions of conductivity with temperature and field. [For example, Eq. (1.5) implies that for $d=2$, the fluctuations in log conductivity should grow as $T^{-1/9}$ upon reducing temperature.] Actually, both assumptions can be questioned. Equations (1.5)–(1.7) provide a correct description of macroscopic conductivity, *if* indeed the variations in a single tunneling event (the critical resistor) dominate the resistivity of the sample. It is more difficult to account for the overall behavior if the contributions of many resistors are important.[27,30,18] Equation (1.1) also breaks down in the presence of Coulomb repulsions.[19] Naively, one might expect to use the same results, but with the dependence appropriate to the presence of a Coulomb gap [e.g., $t\sim T^{-1/2}$ in $d=3$ (Ref. 19)]. However, interactions can also modify the universality classes in ways that we have not explored. (They will most probably introduce a crossover length scale, associated with phase breaking, beyond which the results are not valid.) An even greater impediment is the asymptotic nature of our results, which hold for $t\gg\xi$. This is far from the vicinity of the metal-insulator transition where most measurements are performed. Measuring the variations in the small conductivities of strongly localized electrons will certainly be a challenge for experiments. The most important consequence of our results is providing a *theoretical* understanding of the nature of correlations in the strongly disordered phase.

II. QUANTUM INTERFERENCE OF FORWARD-SCATTERING PATHS

A. The NSS model

The object of this work is to investigate the possible role of coherent QI effects in the VRH regime. This is motivated by clear experimental observations of reproducible conductance fluctuations and positive MC, unexpected in the absence of interference phenomena. The existence of long hops between phase randomizing (phonon scattering) events, extending over many intermediate impurity sites, provides a source for such interference. The hop is no longer a single event but a superposition of many possible multiple-scattering paths between the initial and final sites; intermediate scattering being elastic preserves the phase memory of the electrons (i.e., phase changes are deterministic). The model that is the basis of this work, as proposed by Nguyen, Spivak, and Shklovskii,[27] considers QI for a single resistor in the Miller-Abrahams network,[16] i.e., a single hop. As depicted in Fig. 1, the impurities of this model are placed on a regular lattice. The initial and final impurity sites are on diagonally opposite corners of a square lattice; the intermediate elastic scattering impurities are located at the internal sites (the *site model;* for computational convenience, the impurities are sometimes located at the bonds in a *bond model*). Electrons emerging from the initial site may follow many possible trajectories that lead to the final site. The overall probability amplitude is obtained by the sum of all paths between the two points and includes their quantum-mechanical interference. Quantitatively, the intermediate scattering is governed by an Anderson tight-binding Hamiltonian[1]

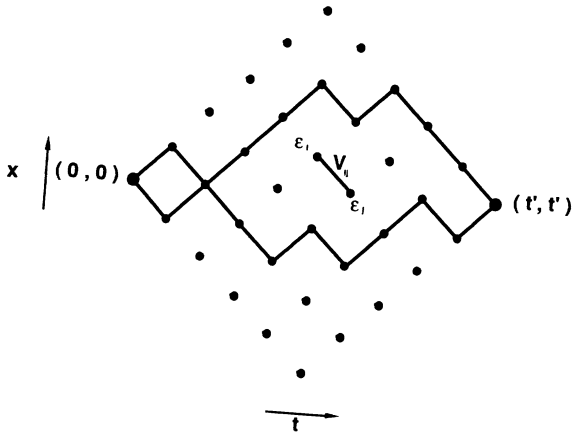

FIG. 1. The NSS geometry used in the simulations. Two directed paths are indicated, connecting (0,0) to $(0,t=2t')$.

$$\mathcal{H}=\sum_i \epsilon_i a_i^\dagger a_i+\sum_{\langle ij\rangle} V_{ij}a_i^\dagger a_j\ , \tag{2.1}$$

where ϵ_i are the site energies and V_{ij} represent the nearest-neighbor couplings or transfer terms. NSS further simplify the problem by choosing site energies distributed according to

$$\epsilon_i=\begin{cases}+W & \text{with probability } p\ ,\\ -W & \text{with probability } (1-p)\end{cases}$$

and a transfer term

$$V_{ij}=\begin{cases}V & \text{if } i,j \text{ are nearest neighbors}\\ 0 & \text{otherwise}\ .\end{cases}$$

We will generally assume $p=\frac{1}{2}$, but will briefly discuss the effects of different p values, presumably emulating the effects of changing the Fermi energy.[27] To describe strong localization, the Anderson parameter is taken to be much smaller than one ($V/W\ll 1$), corresponding physically to a lightly doped semiconductor. This parameter tells us that the width of the band (~ 2 V) centered at energy W is much smaller than its energy difference to the Fermi level.

Using this model, the situation deep in the insulating regime is studied by performing a "locator" expansion;[1] valid in the limit $|V_{ij}|=V\ll(E-\epsilon_i)$, where E is the electron energy. Indeed, for $V=0$, the eigenfunctions are just the single site states, and the localization length is zero (no transfer term). For $V/(E-\epsilon_i)\ll 1$, various quantities can be obtained perturbatively around this solution, as expressed by the Lippman-Schwinger equation[40] in the number representation

$$|\Psi^+\rangle=|\Phi\rangle+\frac{1}{E-H_0+i\delta}\mathcal{V}|\Psi^+\rangle\ . \tag{2.2}$$

The bare Hamiltonian

$$H_0=\sum_i \epsilon_i a_i^\dagger a_i$$

has no nearest-neighbor coupling, while the perturbation

$$\mathcal{V}=\sum_{\langle ij\rangle} V_{ij}a_i^\dagger a_j$$

describes the small transfer terms. $|\Phi\rangle$ represents the state with a localized electron at the initial site (or incident wave), $|\Psi^+\rangle$ the state with a localized electron at the final site. In the coordinate representation, the wave functions are exponentially localized around the impurity sites and there are no propagating waves, since electrons can only tunnel under a potential barrier. (This situation was first addressed in detail by Lifshits and Kirpichenko.[41]) We can now iterate this implicit equation to obtain an expansion in powers of the ratio $\mathcal{V}/(E-\epsilon_i)$ as

$$|\Psi^+\rangle=|\Phi\rangle+\frac{1}{E-H_0+i\delta}\mathcal{V}|\Phi\rangle + \frac{1}{E-H_0+i\delta}\mathcal{V}\frac{1}{E-H_0+i\delta}\mathcal{V}|\Phi\rangle+\cdots . \tag{2.3}$$

Acting with $\langle\Psi^+|$ on the left and taking δ to zero, we obtain the overlap between the two states:

$$\langle\Psi^+|\Psi^+\rangle=\langle\Psi^+|\Phi\rangle+\left\langle\Psi^+\left|\frac{1}{E-H_0}\mathcal{V}\right|\Phi\right\rangle + \left\langle\Psi^+\left|\frac{1}{E-H_0}\mathcal{V}\frac{1}{E-H_0}\mathcal{V}\right|\Phi\right\rangle+\cdots . \tag{2.4}$$

For a more general transfer term $\mathcal{V}$ connecting all sites, the first term represents an electron starting from the initial site and ending at the final site without scattering (the overlap $\langle\Psi^+|\Phi\rangle$); the second term represents electrons scattering *once* off intermediate sites, the third, scattering *twice*, etc. The operator $\mathcal{V}$ acting on $|\Phi\rangle$ produces a factor V for each segment crossed, and H_0 acting on a particular site i results in ϵ_i, the noninteracting site energy. Thus finally we arrive at a simple expression for the amplitude or the Green's function between the initial and final states as

$$\langle\Psi^+|\Psi^+\rangle=\langle\Phi|G(E)|\Psi^+\rangle=\sum_\Gamma\prod_{i_\Gamma}\frac{Ve^{iA}}{E-\epsilon_{i_\Gamma}} . \tag{2.5}$$

Note that we have also introduced a magnetic vector potential defined on the bonds; its effects are treated in the next section.

The terms in the above perturbation series correspond to all paths Γ connecting the end points; i_Γ label the sites along each path. In the NSS model[27] the site energies are $\epsilon_i=\pm W$ with equal probability, while the initial and final impurities have practically the same energy, equal to the Fermi energy; hence without loss of generality we set $\epsilon_F=E=0$. All the energy denominators in Eq. (2.5) now contribute the same magnitude W, but random signs $\eta_{i_\Gamma}=\epsilon_{i_\Gamma}/W$. A path of length l now contributes an amplitude $W(V/W)^l$ to the sum, as well as an overall sign. In the localized regime, the sum is rapidly convergent, dominated by its lowest-order terms.[1] In general, the sum is bounded by one in which all terms make a *positive* contribution, i.e., by a lattice random walk that is convergent for $z(V/W)<1$, where z is the lattice coordinate number. This provides a lower bound for the delocalization transition, and the series is certainly convergent for smaller values of V/W. In the random-walker problem, loops become important only after the transition, while for values of $(V/W)<1/z$ there is a maximum size for typical loops set by a finite correlation length ξ. For distances larger than ξ, it is sufficient to examine directed paths. We expect a similar picture to hold for Eq. (2.5), with ξ the localization length. With $(V/W)\ll 1$, the localization length is less than a single lattice spacing, and only directed (*forward-scattering* paths) need to be considered. Loops (*backscattering* paths) are irrelevant in the renormalization-group sense. This reduction to shortest paths is a considerable simplification and allows efficient numerical study of the strongly localized regime. For sites separated by a distance t along a diagonal of the square lattice, Eq. (2.5) is now simplified to

$$\langle i|G(E)|f\rangle=\left[\frac{V}{W}\right]^t J(t) , \qquad J(t)=\sum_{\Gamma'}^{\text{directed}}\prod_{i_{\Gamma'}}\eta_{i_{\Gamma'}}e^{iA} ; \tag{2.6}$$

the sum is now restricted to the subset Γ' of shortest paths, two of which are indicated in Fig. 9 [corrections are $\mathcal{O}(V/\epsilon)^{t+2}$]. All the interference information is now contained in $J(t)$. The geometry chosen by NSS maximizes possible interference by having a large number of shortest paths. For tunneling along the sides, rather than the diagonal, of a square lattice, there is only one shortest path. Then including longer paths with kinks is essential to the interference phenomena. However, the analogy to random walks suggest that the universal behavior is the same in the two cases: the approach to asymptotic behavior is much slower in the latter. These issues will be further discussed in Sec. V.

B. Numerical results

For each realization of randomness, the contribution of forward-scattering paths to $J(t)$ in Eq. (2.6) can be computed exactly using a *transfer-matrix method.* Let $J(x,t)$ denote the sum over all such paths from (0,0) to (x,t) (see Fig. 1), including the random sign $\eta_{(x,t)}$. Clearly $J(x,t+1)$ only depends on $J(x-1,t)$, $J(x+1,t)$, and the random sign $\eta_{(x,t+1)}$, and hence can be constructed recursively using

$$J(x,t+1)=\eta_{(x,t+1)}[J(x+1,t)+J(x-1,t)] . \tag{2.7}$$

Although the number of paths contributing to $J(t)\equiv J(0,t)$,

$$\mathcal{N}=\begin{bmatrix} t \\ t/2 \end{bmatrix} \overset{t\ \text{large}}{\simeq} 2^t ,$$

grows exponentially with t, the transfer-matrix procedure calculates the sum is polynomial time. The computation time increases approximately as the volume of the system, since the above recursion relation is invoked once

for each lattice site. Ultimately, the results have to be averaged over many realizations of randomness.

We typically performed numerical computations on systems of up to size $t=2000$, and averaged over 2000 realizations of randomness, on a VaxStation II. The random numbers ($+1$ or -1) were obtained from a well-tested random-number generator,[42] with shuffler. Since J grows exponentially in t, $\ln|J|$ has a well-defined probability distribution; we examined its mean $\langle \ln|J(t)| \rangle$ and variance $\langle \ln|J(t)|^2 \rangle - \langle \ln|J(t)| \rangle^2$ for $p=\frac{1}{2}$ (both signs equally probable). We also computed the typical excursions of the paths in the lateral direction as defined by

$$\langle [x(t)^2]_{\rm av} \rangle = \left\langle \frac{\sum_x x^2 |J(x,t)|^2}{\sum_x |J(x,t)|^2} \right\rangle \tag{2.8}$$

and

$$\langle [x(t)]^2_{\rm av} \rangle = \left\langle \left[\frac{\sum_x x |J(x,t)|^2}{\sum_x |J(x,t)|^2} \right]^2 \right\rangle . \tag{2.9}$$

Here $\langle\ \rangle$ represents averaging over realizations of randomness, while $[\ ]_{\rm av}$ is an average over the lateral coordinate at a fixed t, using a weight $|J(x,t)|^2$. (The lateral excursions where computed on a open geometry.)

The quantity $\ln|J(t)|$ is similar to a quenched average free energy, and we confirmed that as any extensive quantity it grows linearly with t [$\langle \ln|J(t)| \rangle = (0.322 \pm 0.001)t$]. Typical fluctuations for $\ln|J(t)|$, plotted in Fig. 2, show a power-law growth as t^{ω} with $\omega = 0.33 \pm 0.05$ (fitting the asymptotic region). For several choices of t we also checked in detail that $J(t)$ is positive or negative with the equal probability, and that histograms of $\ln|J(t)|$ (the whole probability distribution) are well fitted to Gaussian forms whose average and fluctuations conform with the previous results. For lateral excursions, Fig. 3, we obtained good data from simulations with $t=4000$, and with 200 realizations of randomness [reasonable data for fluctuations of $\ln|J(t)|$ are only obtained from higher averaging]. The results for $\langle [x^2]_{\rm av} \rangle$ and $\langle [x]^2_{\rm av} \rangle$ seem to converge to a common asymptotic limit; our fit corresponds (dashed line in Fig. 3) to a power law $t^{2\nu}$ with $\nu = 0.68 \pm 0.05$. The difference between the latter quantities is also depicted, and $(\langle [x^2] \rangle - \langle [x]^2 \rangle)^{1/2}$ grows as $t^{1/2}$, a subleading power law.

We interpret these results as due to a distribution of $|J(x,t)|^2$ with a width growing as $t^{1/2}$, while its center fluctuates as t^{ν}. As discussed in the next section, this behavior is reminiscent of the fluctuation of directed polymers in random media.[43,44] For directed polymers, fluctuations of the "center" can be visualized as stretchings of a coarse-grained path length by x^2/t. The associated energy cost of stretching is tolerated if sufficient free-energy fluctuations are available.[44] As the free-energy fluctuations increase like t^{ω}, this implies the exponent identity[44] $2\nu - 1 = \omega$, consistent with our numerical results; $\omega \approx \frac{1}{3}$ and $\nu \approx \frac{2}{3}$. However, using a similar procedure, Zhang[45] concluded from fits to his numerical results a value of $\nu \approx 0.74 \pm 0.01$. Using a variety of theoretical arguments,[45] he suggests $\omega = \frac{1}{2}$ and $\nu = \frac{3}{4}$. The value of $\omega = \frac{1}{2}$ is clearly consistent with our data, while

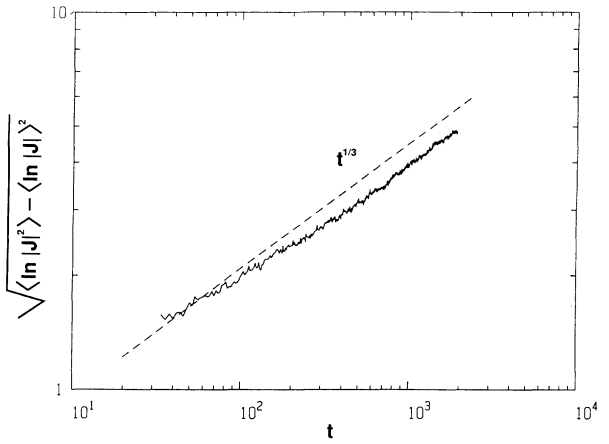

FIG. 2. Standard deviation of the logarithm of the sum over directed paths vs the path length t. The dashed line has a slope of $\omega = \frac{1}{3}$. (Disorder averaging is denoted by the angular brackets.)

$\nu = \frac{3}{4}$ can be obtained if one fits only to $\langle [x]^2_{\rm av} \rangle$. More recently, Gelfand[46] has resolved this conflict by performing highly averaged simulations on smaller lattices. The most important ingredient of his analysis is the inclusion of corrections to leading scaling. The results of Gelfand are completely consistent with our estimates, and again rule out the proposed values of Zhang.[45]

C. Analytical results

Analytic information about the probability distribution can be extracted[47] by examining the moments $\langle J^n \rangle$ and the related characteristic function for $\ln|J(t)|$. As each term in J describes a path traversing the random medium, terms in J^n correspond to the product of contributions from n independent paths. Upon averaging, if m paths cross a particular bond ($0 \le m \le n$), we obtain a factor of $[1+(-1)^m]/2$, which is 0 or 1 depending on the parity of m. For odd n there must be bonds with m odd, and hence $\langle J^{2n+1} \rangle = 0$; which, of course, implies

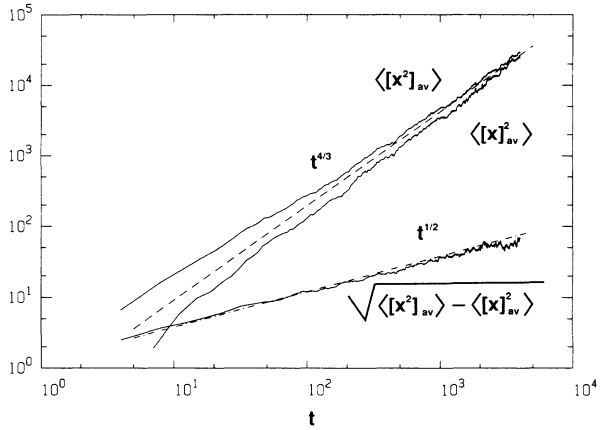

FIG. 3. Transverse fluctuations measured by $\langle [x^2]_{\rm av} \rangle$ and $\langle [x]^2_{\rm av} \rangle$ vs the path length t. The dashed line has slope $2\nu = \frac{4}{3}$. The difference between the two curves appears to grow linearly in t. The dashed-dotted line has a slope of $\frac{1}{2}$.

and follows from the symmetry $P(J)=P(-J)$. For even moments $\langle J^{2n}\rangle$, the only configurations that survive averaging are those in which the $2n$ replicated paths are arranged such that each bond is crossed an even number of times. The simplest configurations satisfying this constraint correspond to drawing n independent paths between the end points and assigning two replica indices to each. The above constraint is also satisfied by forming groups of four or higher even numbers, but such configurations are entropically unlikely, and we shall henceforth consider only paired paths. There is an important subtlety in calculating $\langle J^{2n}\rangle$ from the n paired paths: After two such paths cross, the outgoing paths can either carry the same replica pair labels as the ingoing ones, or they can exchange one label [e.g., (12)(34)→(12)(34), (13)(24), or (14)(23)]. Therefore, there is a multiplicity of three per crossing of paths, which means that such intersections are statistically favored. This can be regarded as an attraction between paired paths induced by the exchange of a replica partner.

Calculating $\langle J^{2n}\rangle$ is now reduced to finding the sum over n paired paths attracted to each other by a factor of 3 per crossing. Its functional form is most easily calculated in a continuum limit by regarding the paths as world lines of n attracting particles in one dimension described by a Hamiltonian[47]

$$-\mathcal{H}_n = n\ln 2+\gamma\sum_{\alpha=1}^{n}\frac{\partial^2}{\partial x_\alpha^2}+\sigma^2\sum_{\beta>\alpha}\delta(x_\alpha-x_\beta)\ . \tag{2.10}$$

The first term describes the choice of two directions per step; the second term is a kinetic-energy term from particle motion, and γ is an effective line tension (in the NSS model it is entropically generated from the light cone constraints). The last term describes the contact attraction between replicas due to partner exchange. The n-body partition function is then computed as

$$\langle J^{2n}\rangle=\mathrm{Tr}[\exp(-\mathcal{H}_n t)]\overset{t\to\text{large}}{\simeq}\exp(-\epsilon_n^0 t)\ , \tag{2.11}$$

where ϵ_n^0 is the n-body ground-state energy (the largest transfer-matrix eigenvalue), which dominates the long-t statistics. In order to obtain the ground-state energy, we need the ground-state wave function which for this system is given by the well-known Bethe Ansatz

$$\Psi_0=C\exp\left[-\frac{\kappa}{2}\sum_{\beta>\alpha}|x_\alpha-x_\beta|\right]\ , \tag{2.12}$$

where C is a normalization constant. To ensure that Ψ_0 is an eigenfunction of $\mathcal{H}_n$, we have to match its discontinuities when two particles cross to the strength of the attractive interaction. This requires $4\gamma\kappa=\sigma^2$, and introduces a transverse length scale $l^*=\kappa^{-1}=4\gamma/\sigma^2$. For the continuum approximation to hold, we need $l^*\gg a$, where a is the lattice spacing. Substituting Ψ_0 in the eigenvalue equation yields[47]

$$-\epsilon_n^0=n\ln 2+\frac{\gamma\kappa^2}{6}n(n^2-1)\ , \tag{2.13}$$

where $\gamma\kappa^2/6\equiv\rho$ is a positive constant. Hence, for large t, $\langle J(t)^{2n}\rangle\sim 2^{nt}e^{\rho n(n^2-1)t}$, as in Eq. (1.3). (Note that the moments of J^2 grow faster than $n!$, thus violating the conditions for attaining a unique probability distribution; this does not necessarily mean that a universal distribution does not exist, as discussed in Sec. V.) However, by definition, cumulants C_i of the characteristic function for $\ln J^2$ are obtained from the powers of n in the expression

$$\langle J(t)^{2n}\rangle=\langle\exp[n\ln J(t)^2]\rangle \equiv\exp\left[\sum_i\frac{n^i}{i!}C_i[\ln J(t)^2]\right]\ . \tag{2.14}$$

C_1 is the average, $\langle\ln J(t)^2\rangle$, while the absence of an n^2 term in Eq. (2.13) indicates no second cumulant at order of t. (It does not rule out a subleading power of t for the variance.[48]) The n^3 term reflects a third cumulant scaling as t, i.e.,

$$\begin{aligned}&\langle\ln J(t)^2\rangle=[\ln 2-\rho]t\ ,\\ &C_2[\ln J(t)^2]=0\ (\text{to order } t)\ ,\\ &C_3[\ln J(t)^2]=6\rho t\ .\end{aligned} \tag{2.15}$$

Hence $\ln|J|$ is *approximately* normally distributed: Its average increasing as t, and fluctuations growing as $t^{1/3}$; i.e., $\omega=\frac{1}{3}$, in agreement with numerical simulations. Due to the usual difficulties of mappings between discrete and continuum theories, it is not easy to estimate the parameters γ, σ^2, and hence ρ in general. Based on the reduced value of $\langle\ln|J(t)|\rangle$, we can estimate $\rho_0\approx 0.053\pm 0.002$ for the NSS model in zero field. As noted earlier, the above arguments are almost identical to those presented for directed polymers in a random potential.[47] The conceptual difference is in the origin of the attraction between paths, which in this case is purely a statistical exchange effect. The averaging also introduces multiparticle interactions in Eq. (2.10). In the continuum limit $l^*\gg a$, these interactions should be unimportant, although Zhang[45] has questioned this assumption. They certainly do not modify the results for the directed polymer problem.

The final expression for the full Green's function [Eq. (2.5)] is

$$\langle\ln|\langle i|G|f\rangle|^2\rangle=-\frac{t}{\xi_0}-\rho t\ , \tag{2.16}$$

where

$$\xi_0=\left[2\ln\left[\frac{\sqrt{2}W}{V}\right]\right]^{-1} \tag{2.17}$$

is the *local* contribution to the localization length involving only the Anderson parameter. There is also a *global* contribution $\xi_g^{-1}=\rho$ from the quantum interference information. For the NSS model $\xi_g\approx 20$, and indeed the asymptotic behaviors in Figs. 2 and 3 only become apparent beyond this scale. It is ξ_g that parametrizes the universal aspects of the distribution, and its variations as discussed in the following sections, in particular

$$\delta\ln|\langle i|G|f\rangle|\sim\left|\frac{t}{\xi_g}\right|^{1/3}\ . \tag{2.18}$$

D. The "sign" transition

We have focused so far on the symmetric case of $p=\frac{1}{2}$. In their original paper, NSS (Ref. 27) also raise the possibility of a "sign" transition as a function of p: For small concentrations p of negative signs, the "sign" information is maintained, while for $p>p_c$ positive and negative J are equally likely. The experimental consequence of this sign transition is[27] a change in the frequency of Aharonov-Bohm oscillations from hc/e to $hc/2e$. NSS were led to this conclusion from numerical results on systems of size $t<200$, with over 2000 realizations of randomness, which exhibit a continuous change of the "order parameter" $\Delta P=P(J>0)-P(J<0)$ for impurity concentrations close to $p=0.05$. In this section we briefly review the arguments for and against such a transition, and point out the difficulties of settling this question numerically.

To support the "sign" transition, NSS proposed a simple explanation based on an *independent-path approach* (IPA). The mean value of J is easily calculated as

$$\langle J\rangle=\sum_{\alpha}\langle J_{\alpha}\rangle=\begin{bmatrix} t \\ t/2 \end{bmatrix}\langle J_{\alpha}\rangle\approx 2^{t}(1-2p)^{t}\ . \tag{2.19}$$

The first term is just the number of paths, while the second comes from $\langle \eta_i\rangle=(1-2p)$ for each bond along the path. Similarly, the second moment is given by

$$\langle J^2\rangle=\left\langle\left[\sum_{\alpha}J_{\alpha}\right]^2\right\rangle$$
$$=2^{t}+\sum_{\alpha\neq\beta}\langle J_{\alpha}J_{\beta}\rangle\approx 2^{t}+2^{t}(2^{t}-1)\langle J_{\alpha}J_{\beta}\rangle\ . \tag{2.20}$$

In the IPA approximation, the paths are treated as independent variables. Hence, $\langle J_{\alpha}J_{\beta}\rangle=\langle J_{\alpha}\rangle^2$, so that the fluctuations of J are

$$(\delta J)^2=\langle J^2\rangle-\langle J\rangle^2=2^{t}(1-\langle J_{\alpha}\rangle^2)\approx 2^{t}\ . \tag{2.21}$$

NSS argue that $\langle J\rangle$ is the extent to which "positive" paths exceed "negative" ones in the sum, and that its relative magnitude compared to the fluctuations gives a characterization of the phases: If the phase is dominated by one sign, we expect the average to win out over the fluctuations, and the ratio $\langle J\rangle/\delta J$ to diverge with the size t. On the other hand, if both signs are equally probable, the fluctuations will win over the average, and $\langle J\rangle/\delta J$ vanishes. The boundary between the two behaviors occurs for $2(1-2p)=\sqrt{2}$, i.e., at a $p_c\approx 0.14$ (compared to the numerical estimate of $p_c=0.05$).

Shapir and Wang[49] were the first to criticize the assumption of independent paths. They showed, by computing $\langle J_{\alpha}J_{\beta}\rangle$ more carefully, that corrections to IPA invalidate the argument in that the corrected fluctuations exceed the average for *all values* of p. They thus concluded the absence of a phase-preserving sign information, and the associated hc/e periodicity in oscillations. This is again due to the correlations between paths that lead to the formation of bound states in the computation of moments $\langle J^n(t)\rangle$. We can repeat the analysis of the previous section for general p: As a result of averaging, we obtain a factor of $(1-2p)$ for any odd number of paths through a particular site. Thus for $p\neq\frac{1}{2}$ double occupation is no longer absolutely necessary, although the reduced factor of $1-2p$ for $p\neq 0$ attracts the paths together. For small p we again expect a bound state in which the n replicas appear on the same footing. The result $\langle J^2(t)\rangle\gg\langle J(t)\rangle^2$ merely reflects the formation of the two-particle bound state. However, at $p=\frac{1}{2}$, we have a bound state of pairs, i.e., a dimerization occurs somewhere between $p=0$ and $\frac{1}{2}$. We currently cannot answer whether this is a true phase transition (possibly a reflection of the "sign" transition, or a crossover). A recent study by Wang *et al.*[50] employs an exact enumeration of all impurity configurations, and seems to suggest the absence of a transition. However, such an approach is necessarily limited to small sizes, and the results for $t\leq 10$ may not necessarily reflect the true asymptotics.

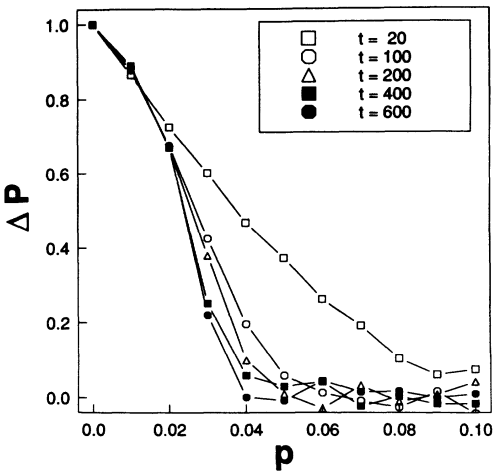

FIG. 4. The dependence of $\Delta P=P(J>0)-P(J<0)$ on p, the probability of $-$ signs, for t up to 600.

We performed simulations of the NSS model close to the proposed transition. We generated systems of size 300×300 ($t=600$), performing 100 realizations of randomness for both the random-site and random-bond models. As the NSS simulations concern the site model, we will also focus on the former. The results for ΔP versus p in Fig. 4 are qualitatively similar to those of NSS for small t. However, the figure clearly indicates that the asymptotic limit does not set in for these sizes. A transition, if one occurs at all, takes place below $p=0.05$. Figure 5 shows a rapid decay of the "order parameter" ΔP with size above $p=0.02$ The characteristic length for these decays becomes progressively larger as p is decreased. A study of much larger systems, and a careful finite-size scaling analysis, is necessary to distinguish between a crossover and a second-order transition with $p_c\approx 0.02$. Further work is in progress.

The observation of only $hc/2e$ oscillations in experiments[25] seems to support the absence of a phase transition. An interesting percolation study by Xie and Das-Sarma[51] shows that the change in frequency of the oscillations from hc/e to $hc/2e$ associated with the sign transition only occurs for finite-size Aharonov-Bohm rings.

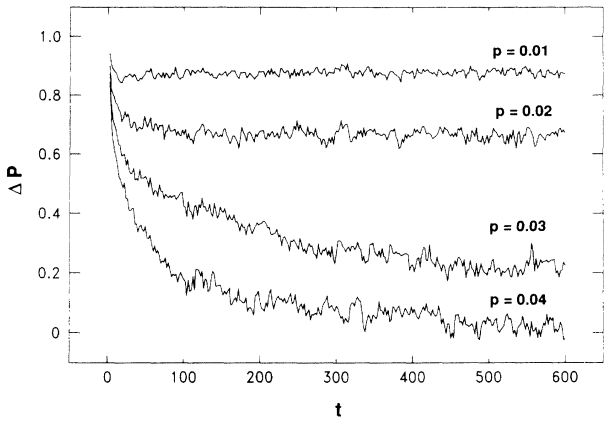

FIG. 5. ΔP vs size t for different values of p. The very slow decay (nonexistent within numerical resolution) for $p=0.01-0.02$ leaves open the possibility of a phase transition.

As the rings increase in size, the critical concentration decreases, approaching zero, with, again, a somewhat slow convergence. Actually, an analytical argument of "mean-field" flavor, and hence probably correct for dimensions $d>4$, by Obukhov,[52] does support the existence of a "sign" transition. Its absence in our numerical simulations may indicate that the lower critical dimension for this transition must exceed two.

III. MAGNETIC-FIELD RESPONSE

A. Tunneling under a pure potential

Before describing the effects of a magnetic field on localized electrons, we briefly describe its influence on tunneling under a uniform lattice potential. The intriguing behavior of electrons on a lattice subject to an external magnetic field has captured the attention of many physicists. Many of the unusual behaviors originate in the incommensurability of the magnetic length with the lattice spacing.[35,53] Hofstadter,[38] for example, describes in great detail the band structure of noninteracting electrons, and the generalized Bloch states in a magnetic field. In this section we consider a different regime of the same problem. A state localized near an impurity site, with an energy deep in the gap of the bulk spectrum. For a gap state, one expects an exponential decay of the wave function into the bulk, but we shall demonstrate that the decay of the wave function exhibits an interesting dependence on the field.

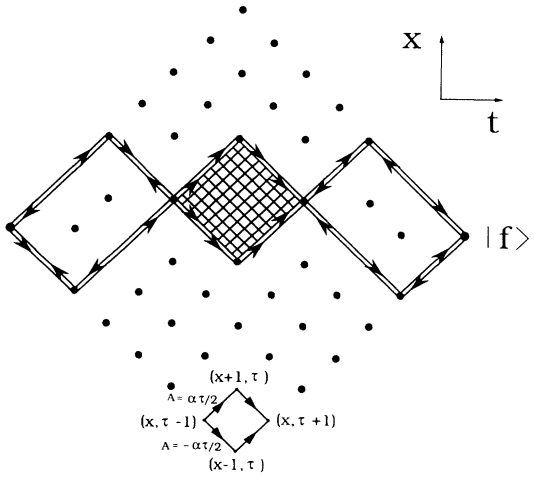

FIG. 6. NSS geometry in a magnetic field, and the "diagonal staggered gauge." Directed paths of length t are paired by the randomness averaging. Right- (left-) pointing arrows indicate paths from J (J^*).

We again start with the NSS model, but this time all the intermediate energies are equal ($\epsilon_i=+W$ for all i, except for the initial site, which has zero energy). A magnetic field is introduced through the phase of the overlap terms, i.e., $V\rightarrow Ve^{iA}$, where A is the gauge potential. We chose the "diagonal staggered gauge" as depicted in Fig. 6 with $A(\tau)=\pm\alpha\tau/2$, where $\alpha=2\pi\phi/\phi_0$ is the fractional flux per plaquette. With this choice, the transfer matrix has no x dependence, but depends on t. Equation (2.7) can now be generalized, and written in matrix form as $J(\tau+1)=T(\tau)J(\tau)$, with a transfer matrix

$$\langle x|T(\tau)|x'\rangle=\exp\left[\frac{-i\alpha\tau}{2}\right]\delta_{x,x'+1}+\exp\left[\frac{i\alpha\tau}{2}\right]\delta_{x,x'-1}\,. \tag{3.1}$$

As Fig. 7 indicates, the amplitude for tunneling a dis-

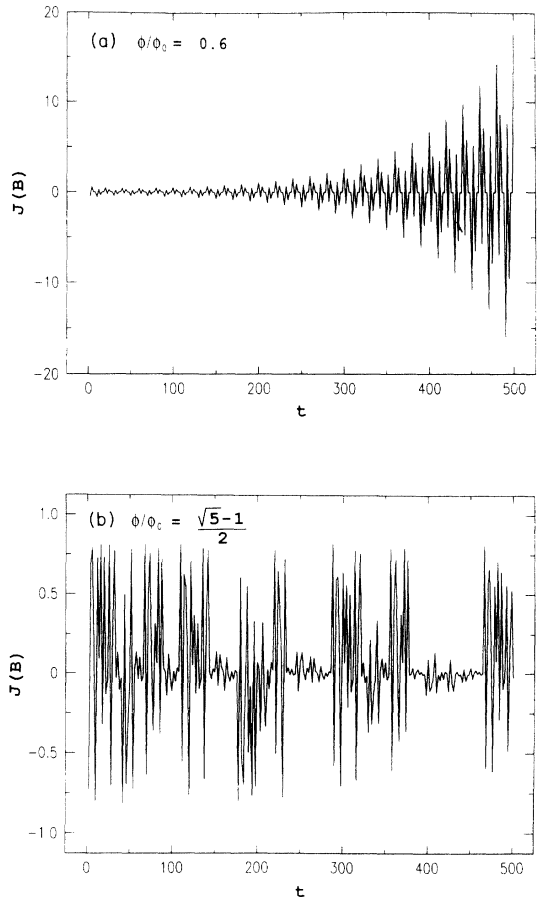

FIG. 7. Behavior of $J(B,t)$ for large fields. The flux per plaquette is (a) rational, $\phi/\phi_0=0.6$, and (b) irrational, $\phi/\phi_0=(\sqrt{5}-1)/2$ (the golden mean).

tance t is very sensitive to the commensurability of the flux per plaquette. For rational values of ϕ/ϕ_0, $J(t)$ exhibits a regular pattern, and is in fact very large at special values of t. On the other hand, for an irrational ϕ/ϕ_0 it seems to randomly fluctuate between -1 and $+1$.

The diagonal staggered gauge also has the advantage that the transfer matrices at different τ slices commute ($[T(\tau),T(\tau')]=0$), and are hence simultaneously diagonalizable. This is accomplished in a Fourier basis, and the eigenvalues are

$$\lambda_p(\alpha,\tau)=2\cos\left[\frac{\alpha\tau}{2}-p\right], \tag{3.2}$$

where p labels the transverse momentum channels. Finally, we obtain

$$J_B(x,t)=\left\langle x\left|\prod_{\tau=1}^{t}T(\tau)\right|0\right\rangle = \sum_p\prod_{\tau=1}^{t}2\cos\left[\frac{\alpha\tau}{2}-p\right]\exp(-ipx) \tag{3.3}$$

and

$$J(B,t)\equiv J_B(0,t)=\sum_p\prod_{\tau=1}^{t}2\cos\left[\frac{\alpha\tau}{2}-p\right], \tag{3.4}$$

which is, of course, an exact sum of *forward-scattering paths* in the nonrandom problem. From Eq. (3.4) we can identify a number of distinct behaviors: For small fields such that less than one flux goes through the entire "sample" (between the hopping end points), the arguments of the cosines are small (focusing on small p values), and

$$J\approx\sum_p\prod_\tau\left[1-\frac{(p-\alpha\tau/2)^2}{2}\right] \approx\sum_p\exp\left[-\frac{1}{2}\sum_\tau\frac{(p-\alpha\tau/2)^2}{2}\right].$$

In the continuum limit we arrive at

$$J\approx\int dp\exp\left[-\frac{1}{2}\left[p^2t-\frac{\alpha pt^2}{2}+\frac{\alpha^2t^3}{12}\right]\right].$$

The sum is dominated by its saddle point at $p^*=\alpha t/4$, which implies

$$\ln J(B)=-\frac{\alpha^2t^3}{96}\sim -B^2t^3 . \tag{3.5}$$

This is the well-known harmonic shrinkage of the wave function.[19] The t^3 dependence can be justified since typical forward-scattering paths are random walks with transverse fluctuations $\delta x\sim t^{1/2}$. Hence, the relevant flux grows as $Bt^{3/2}$. As noted earlier, the behavior of $J(B,t)$ for large fields (when many flux units penetrate the sample) is more complicated and crucially dependent on whether or not the flux per plaquette is rational. In the rational case, $\alpha=2\pi p/q$, there is a periodicity in the sense that a segment of length $\Delta t=4q$ is repeated except for a scaling factor. From Eq. (3.4) it can be shown that the scale factor grows as

$$|J(t)|\sim\frac{1}{\sqrt{t}}2^{t/q} . \tag{3.6}$$

This is completely consistent with the observed behavior for $\phi/\phi_0=\frac{3}{5}$ in Fig. 7(a). We can currently make no statements about the nature of the correlations for irrational ϕ/ϕ_0 as in Fig. 7(b). The patterns are random in appearance, but certainly deterministic.

There is an important point that needs to be addressed here. It is well known from the solution of the Schrödinger equation in a magnetic field that, far from an impurity site, the electron wave function decays with a Gaussian tail, and not as an exponential. (This is due to the harmonic well created by the field.) We do not know if a similar result holds on a lattice. The above exact summation of forward-scattering paths certainly implies an envelope with exponential decay. If it is indeed the case that the true envelope must have a Gaussian decay on a lattice, then the correct answer must require the addition of loops and backscattering. Would this also invalidate the results of the next section, which sum only forward-scattering paths, but in a random potential? Actually, this question has been considered by Shklovskii and Efros,[54] who conclude that the decay should be a simple exponential due to the "shifting" of the quadratic potential created by the field at each of the impurities elastically scattering the electron. Further work is needed to clarify these crucial points.

B. Numerical results

With disorder, we used the procedures outlined in Sec. I B to construct histograms for $P[|\ln|J(B,t)|]$. Note that as J becomes complex in a field, we use its absolute magnitude. A typical histogram is plotted in Fig. 8. In the presence of the magnetic field the distribution becomes sharper, while its mean is increased (indicating enhanced tunneling and a positive MC). We also find that for a field B, $P[\ln|J(B,t)|]$ maintains its functional form in that its mean scales linearly with t and fluctuations grow as $t^{1/3}$. This implies that a magnetic field causes an increase in the localization length. This is more apparent

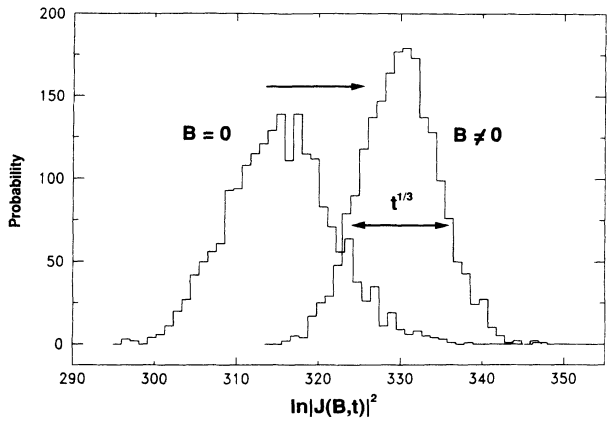

FIG. 8. Histograms for the variable $\ln|J(B,t)|$. A magnetic field increases the average of the probability distribution. The fluctuations decrease while still scaling as $t^{1/3}$ for any fixed field.

in Fig. 9, where as a measure of MC we have plotted $\Delta\langle \ln|J(B,t)|\rangle \equiv \langle \ln|J(B,t)|\rangle - \langle \ln|J(0,t)|\rangle$. The slope of the linear increase in t reflects the change in the localization length $[\rho(B)=\xi_g^{-1}]$. There are actually subleading corrections to the linear scaling of $\Delta\langle \ln|J(B,t)|\rangle$ which are apparent from our data for small sizes. One expects on general grounds[48,56] that the leading dependence of this quantity is linear (i.e., extensive), while the first subleading term grows as $t^{1/3}$; the exponent found for the scaling of the third cumulant. This was suggested by Bouchaud and Orland,[48] who generalized the Bethe Ansatz arguments of Sec. II C to include gapless excitations of the bound-state center of mass. Figure 10 shows a large simulation ($t=4000$ and 1000 realizations of randomness) for the quantity $\Delta\langle \ln|J(B,t)|\rangle$ with $B=10^{-4}$. A very good fit is achieved in the range $t>200$ using the $t^{1/3}$ correction. This is an additional indication that the NSS model and the classical directed polymer problem with positive randomness are in the same universality class.

The observed behavior is consistent with a reduction in the parameter ρ in Eq. (2.15), hence an increase in the *global* contribution to the localization length. The numerical results in fact indicate

$$\xi_g^{-1}=\rho(B)=(0.053\pm0.02)-(0.15\pm0.03)(\phi/\phi_0)^{1/2}\ . \tag{3.7}$$

This suggests the possibility of collapsing the numerical results for different values of t and B by using a universal scaling function $J(B,t)=f(Bt^2)$. This collapse is clearly seen in Fig. 11 for small fields ($\phi \ll \phi_0$). The physical implication is that the characteristic area relevant to this regime scales as t^2, rather than a portion of it. The latter was suggested by NSS,[27] who proposed a scaling $Bt^{3/2}$ as in Eq. (3.5) based on the "cigar-shaped" area covered by random walks. The $B^{1/2}$ dependence was recently reproduced by Zhao *et al.*,[29] who also confirmed its universality by changing the relative probabilities of the random signs and shifts in the Fermi level.

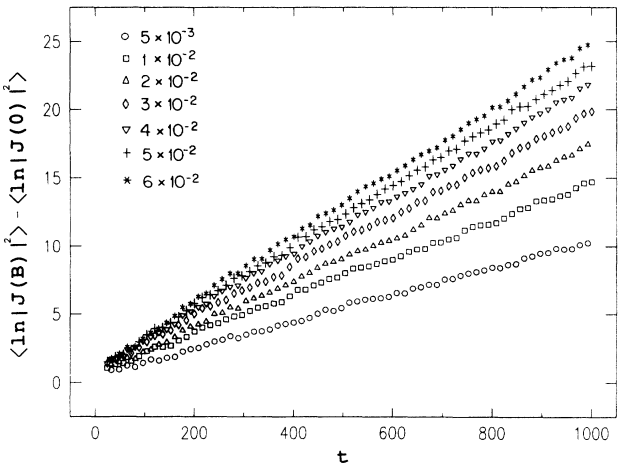

FIG. 9. The magnetoconductance (log-averaged value of the sum of directed paths relative to $B=0$) versus the length t. All fields are measured in units of elementary quantum flux per plaquette.

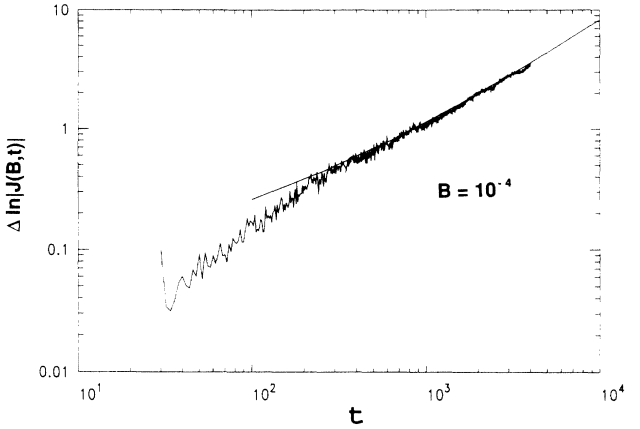

FIG. 10. A fit to the magnetoconductance $\Delta\langle \ln|J(B,t)|\rangle$ (for $B=10^{-4}$), taking into account the subleading scaling as described in the text ($\Delta=\alpha t+\beta t^{1/3}$). The parameters used, $\alpha=0.0074$ and $\beta=0.04$, are field dependent.

The field values leading to the results reported above are much larger than typical experimental values.[23] It is also interesting to inquire at what fields the $B^{1/2}$ dependence breaks down. (Because of the $B\rightarrow -B$ symmetry, and the required analyticity of a finite t system, a B^2 dependence at very small fields is expected.) We therefore performed simulations in the very-low-field regime (10^{-4}–10^{-7} flux quanta per plaquette and $1-10^{-3}$ for the whole system). Reliable results required the very high averaging of around 10 000 realizations of randomness, and appear to be quite sensitive to finite-size effects. Figure 12(a) shows data obtained for samples of 50, 200, and 400×400, and exhibits three well-defined regions. The highest-field values correspond to the above $B^{1/2}$ scaling, there is an intermediate region scaling almost linearly, and finally an incipient B^2 dependence emerges. With increased size t, the $B^{1/2}$ regime extends into smaller fields while the B^2 region almost disappears. We found that the low-field data can best be collapsed by plotting $\Delta\ln|J(B,t)|$ versus $Bt^{3/2}$, and that a crossover occurs for $Bt^{3/2}\approx 1$. Clearly this collapse does not work at higher fields where $\Delta\ln|J(B,t)|\propto B^{1/2}t$. We attempted to collapse the data in both regimes using a single homo-

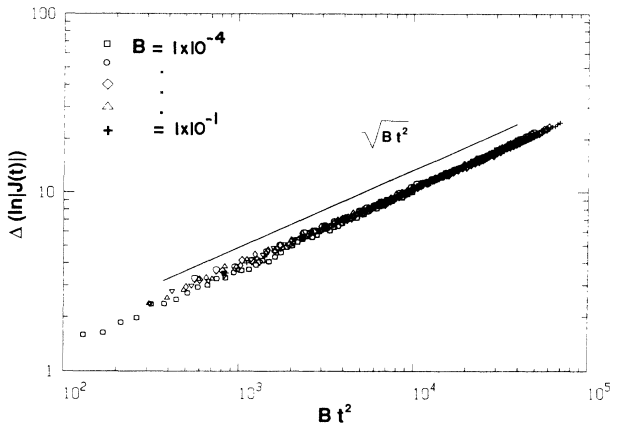

FIG. 11. Data collapse of MC for different fields and sizes indicating a scaling of the form $J(B,t)=f(Bt^2)$.

geneous function of the form $\Delta\ln|J(B,t)| \propto t^x\phi(Bt^y)$, with $x+y/2=1$ for the correct large-B limit. We found no satisfactory collapse of this form, indicating that there may be other relevant length scales. More effort in this direction is in progress.

For a single realization of randomness, the NSS model shows the type of reproducible conductance fluctuations first seen in the VRH regime by Poyarkov *et al.*[25] and Orlov and Savchenkov[20] and confirmed since by others.[21,26] By studying the autocorrelation function as suggested by NSS[27]

$$f(\delta B)=\sum[\ln|J(B+\delta B,t)|\ln|J(B,t)|]-[\ln|J(B,t)|]^2 , \tag{3.8}$$

one can obtain the characteristic period of the fluctuations along the field axis B_c, and hence the effective area directly. Is this area the whole sample, or a fraction of it enclosed by dominant paths? Milliken and Ovadyahu[26,21] seem to confirm the $B_c \sim t^{-3/2}$ scaling proposed by NSS.[27] We also numerically examined these fluctuations by computing autocorrelation functions for small systems of up to $t=162$, and 1000 realizations of randomness (these are extremely time consuming due to the Fourier-transform operation for each realization). The results depicted in Fig. 13 show two distinct regions: The data at the larger fields show autocorrelations decaying as $B^{-2/3}$ for at least two decades, while the data at lower fields cannot be fitted to a power law and may be nonuniversal. The characteristic field scale for this crossover can again be determined by collapsing the various curves after appropriate scaling. The best collapse, shown in Fig. 13(b), was achieved by scaling the Fourier-transform amplitude by $t^{4/5}$, and the abscissa by $Bt^{3/2}$. Translating the latter variable to temperature dependence, using Eq. (1.1), we find good agreement with the experimental findings of Milliken and Ovadyahu.[26] It is, however, quite likely that the larger fields in Fig. 13 still correspond to the intermediate fields in Fig. 12, and that another crossover occurs for larger fields.

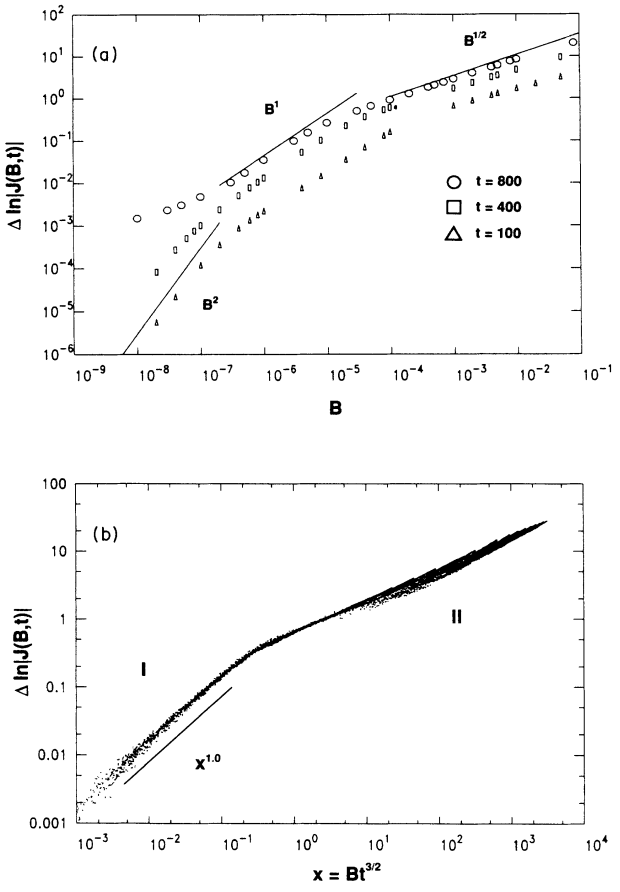

FIG. 12. (a) Highly averaged runs revealing various power-law dependencies of MC on the field. For B approaching 10^{-2} quantum fluxes per plaquette, the $B^{1/2}$ dependence is regained. (b) Data collapse for 20 different field values (from $B=10^{-7}$ to 10^{-1}) using the scaling variable $x=Bt^{3/2}$. While the low-field data scale very well, the higher-field data are less well described. Only systems of sizes $t>20$ are included.

C. Analytical results

The usual explanation for a positive MC, close to the localization transition, relies on the decreased weight of backscattering paths.[6,11] Since our formulation explicitly

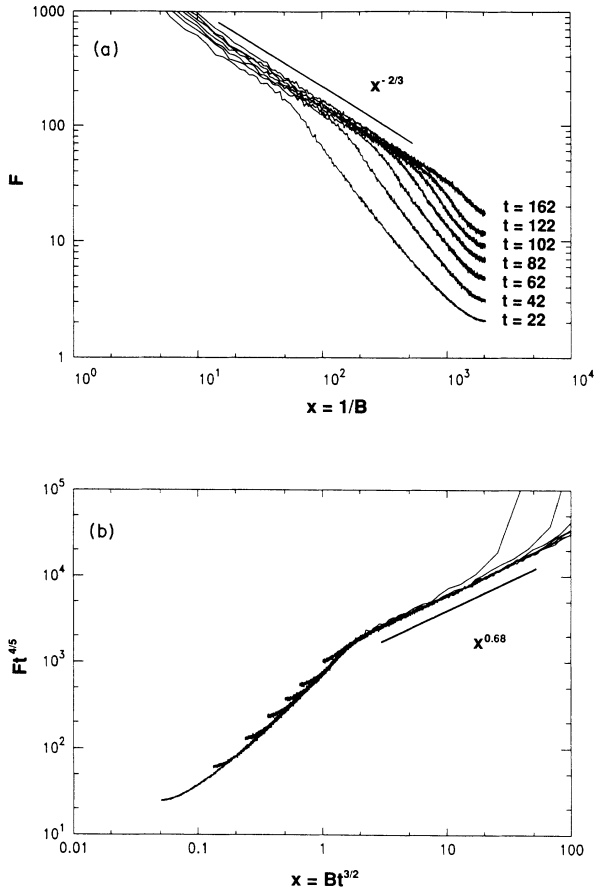

FIG. 13. Top: the Fourier transform of the autocorrelation function. The straight line represents $B^{2/3}$. Bottom: collapse of the same data.

excludes such paths, an alternative explanation is necessary. Such explanations have been offered in the context of forward-scattering paths[27,30] using an independent-path approach. As we shall describe later, the IPA approximation leads only to an overall increase in MC by a factor of 2 and no change in the localization length, in clear contrast to the results in Fig. 9. In the previous section, we established that to properly understand the numerically measured shape of $P[\ln|J(0,t)|]$, it is essential to keep track of the correlations between paths. In this section we extend the replica analysis that achieved this goal to include magnetic-field effects.

In a magnetic field, the sum J becomes complex due to the gauge phase factors, and tunneling probability depends on $|J|^2$. Hence, we examine the moments $\langle (JJ^*)^n \rangle$, which form the appropriate generating function for the cumulants of $\ln|J(B,t)|^2$. $\langle (JJ^*)^n \rangle$ describes configurations of $2n$ paths, n from J and n from J^*, labeled, respectively, in Fig. 6 by arrows pointing to the right and left. Averaging over the random-site energies again pairs up the paths, but two types of pairings can now be distinguished (see Fig. 6): (i) Partners are taken, one from J and one from J^*. Such pairs (referred to as neutral) do not feel the field, since the phase factors of e^{iA} picked up by one member on each bond are canceled by the conjugate factors e^{-iA} collected by its partner, resulting in no pet coupling to the field. (ii) Both partners are taken from J or from J^*. Such paths (referred to as charged) feel a strong interference from the field corresponding to gauge factors of $e^{\pm 2iA}$ (like particles of charge $\pm 2e$). It is reasonable to assume that because of their strong self-interference, charged path of long length do not contribute appreciably to $\langle (JJ^*)^n \rangle$ and that dominant contributions come from neutral paths [this can be readily justified by invoking Eq. (3.4)]. However, between successive intersections of two neutral paths, short segments of charged paths can be present, as indicated in Fig. 6. The intermediate (hatched) loop in this figure can be labeled by the four replica indices in six possible ways, two of which correspond to charged paths. At zero field all six configurations are equally likely, resulting in an exchange multiplicity of 3 (two intersections). For $B \neq 0$, if the area enclosed between intersections is $\mathcal{A}$, the relative contribution of the charged paths is smaller by $\cos(2B\mathcal{A})$, leading to an overall multiplicity factor of $2+\cos(2B\mathcal{A})$ per crossing. This is a decrease in the attraction from its value in the absence of a magnetic field. The net effect of integrating out charged segments is thus to reduce the effective attraction between neutral pairs. This leads to a reduction in the binding energy ρ in Eq. (1.3), simultaneously increasing the mean, and decreasing fluctuations as in Eq. (2.15). In fact, since Eq. (1.3) represents a one-parameter distribution, the changes in mean and variance should be perfectly correlated. This has indeed been tested numerically, as will be described in the next section.

According to the Bethe Ansatz calculations of the previous section, the binding energy ρ is proportional to the square of the attraction $\sigma^2=2+\cos(2B\mathcal{A})$. Hence, for small fields,

$$\delta\rho/\rho=2\delta\sigma^2/\sigma^2=-4\frac{(B\mathcal{A})^2}{3} . \tag{3.9}$$

To proceed further, we need an estimate of the typical area $\mathcal{A}$. The only B-dependent intrinsic length in the problem is the magnetic length $L_B \propto B^{-1/2}$. The choice of $\mathcal{A} \propto L_B^2$ is probably valid at large B, and describes saturation with ρ independent of B. At smaller fields, another possibility is $\mathcal{A} \propto L_B^{3/2} \propto B^{-3/4}$, i.e., the area covered by typical random walks[27] of length L_B. This choice, inserted in Eq. (3.9), leads to the observed field dependence in Eq. (3.7). As noted earlier, the $B^{1/2}$ increase of the localization length has recently been confirmed by Zhao *et al.*[29] They also argue that L_B is the only relevant length scale, subdivide the system in units of size L_B, and propose an increase of tunneling per each unit. Although, this explanation also leads to the correct conclusion, we emphasize that a complete argument must simultaneously account for the scaling of MC *and its fluctuations.* Since Zhao *et al.*[29] argue that the $B^{1/2}$ dependence breaks down for $Bt \sim 1$, the low-field results of Fig. 12 provide another test for such arguments.

A finite magnetic field breaks time-reversal symmetry by introducing complex phases for each path. An extreme limit of this breakdown can be achieved by replacing the sign ($\pm$) randomness with phase randomness ($e^{i\theta}$ with $0<\theta<2\pi$ picked from a uniform distribution). We also simulated the latter model and found that, as expected, it shows no MC (Fig. 14). This result is easily explained in the replica language: In calculating $\langle (J^*J)^n \rangle$, only the neutral paths survive the averaging over θ, since $e^{i\theta(m-m')}=\delta_{m,m'}$, and such paths do not couple to the magnetic field. The charged bubbles, as in Fig. 6, are now totally eliminated and the exchange attraction is reduced to 2 [since $(11^*)(22^*) \rightarrow (11^*)(22^*)$ or $(12^*)(21^*)$]. The random-phase model describes a Hamiltonian with lower *unitary* symmetry (as opposed to the *orthogonal* symmetry of the original model in zero field). It may describe magnetic impurities that break time-reversal symmetry.[57]

The tunneling problem in a magnetic field thus interpolates between the orthogonal and unitary symmetries, but it is never fully equivalent to the latter, as implicitly as-

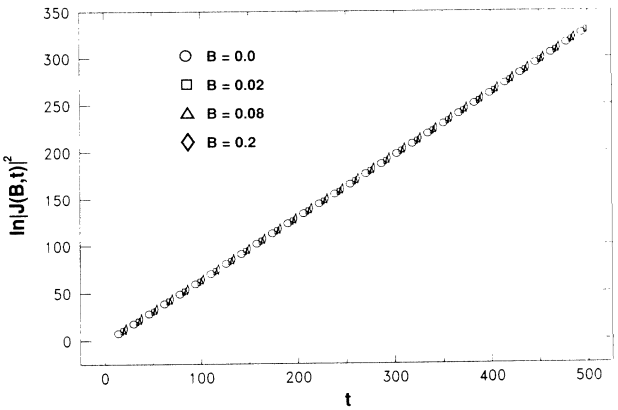

FIG. 14. Numerical demonstration of the field independence of the log-conductance in the presence of random phases. This case corresponds to a Hamiltonian of unitary symmetry due to magnetic impurities.

sumed in the random-matrix approaches.[12,32] This is because the information in the phase of the tunneling amplitude can be used to reconstruct the positions of the impurities. With impurity energies at $\pm\epsilon$, it is clear that the average $\langle J^2(B,t)\rangle$ represents configurations of a paired path of charge $2e$ in a uniform system, i.e., $\langle J^2(B,t)\rangle = J_P(2B,t)$, where in J_P all impurities have the same energy ϵ. This identity was tested numerically for the NSS model as depicted in Fig. 15. We observe that the oscillations of $J(B,t)$ reported in Sec. III A, for tunneling under a uniform potential, can actually be seen for the random system, but only after sufficient averaging.

We conclude this section by discussion the shortcomings of the IPA (Refs. 27 and 30) in calculating the MC. As each contribution to J is treated as independent, $P[J]$ is Gaussian in this approximation. The number of independent elements of J (real or imaginary) changes in a magnetic field. This hypothesis leads[30] to a quadratic-field dependence for small fields (less than 0.1 flux quantum through the whole system) and a saturation at high fields to a typical value of $|J|^2$ larger by a factor of 2. This approach predicts no change in the localization length, which we believe is due to its neglect of correlations between paths. To emphasize this point, we shall rederive the IPA result using a replica analysis of $\langle (J^* J)^n\rangle$. Since the paired paths are regarded as independent, this average in the IPA is simply $A(n)2^{nt}$, where $A(n)$ is the number of possible pairings. (Intersections between paths are thus ignored.) All pairings of $2n$ paths contribute equally at $B=0$ so that $A(n) = 1\times 3\times\cdots\times(2n-1)=(2n-1)!!$. Only neutral paths survive at finite field and $A(n)=n\times(n-1)\times\ldots=n!$. From this information, the log-averaged MC is obtained as

$$\langle \ln|J(B)|^2-\ln|J(0)|^2\rangle = \lim_{n\to 0}\left\langle \frac{|J|^{2n}(B)-|J|^{2n}(0)}{n}\right\rangle = \lim_{n\to 0}\frac{n!-(2n-1)!!}{n} = \ln 2 , \tag{3.10}$$

the increase calculated by Sivan, Entin-Wohlman, and Imry.[30] We thus see that it is precisely the intersection factors, representing the correlations between paths, that are responsible for the global contribution to the localization length ξ_g^{-1}, and its variations in a field.

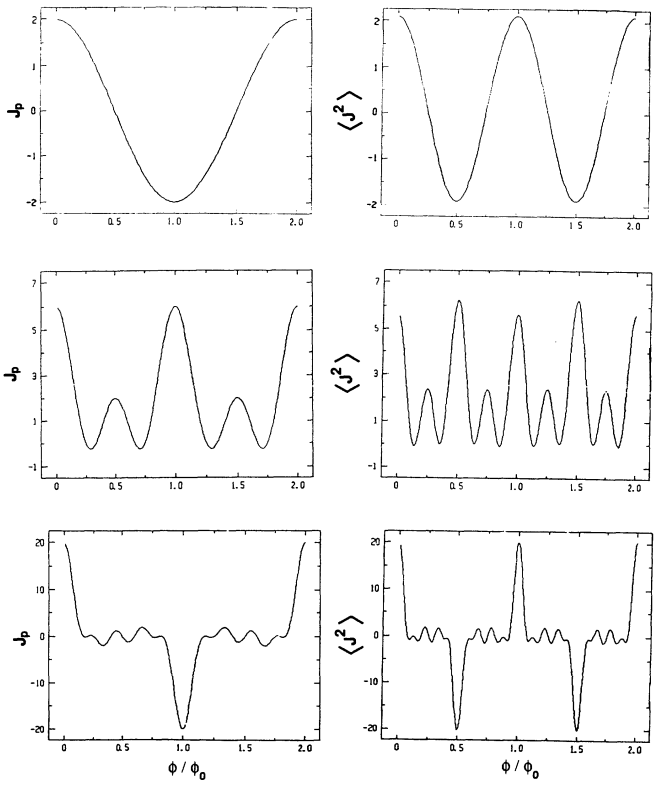

FIG. 15. Numerical verification of the relation $\langle J^2(B,t)\rangle = J_p(2B,t)$ derived from replica theory. J_P describes tunneling under a uniform potential as in Fig. 7. ϕ_0 is the elementary flux quantum and ϕ the flux per plaquette. The curves correspond to values of $t=2$ (top), 4 (middle), and 6 (bottom). The results for $\langle J^2\rangle$ where obtained by averaging about 50 realizations of randomness.

IV. SPIN-ORBIT SCATTERING

A. Numerical results

In the weakly localized regime, *spin-orbit* (SO) scattering has antilocalizing effects,[11] as its destructive interference may dominate the coherent backscattering. In this section we assess the effect of SO in the strongly localized regime by generalizing the NSS model to include (SO) impurity scattering in addition to the underlying potential scattering ($\pm$ randomness). The starting point is the Hamiltonian

$$\mathcal{H} = \sum_{i,\sigma}\epsilon_i a^\dagger_{i,\sigma}a_{i,\sigma} + \sum_{\langle ij\rangle,\sigma\sigma'} V_{ij,\sigma\sigma'}a^\dagger_{i,\sigma}a_{j,\sigma'} . \tag{4.1}$$

The constant nearest-neighbor-only hopping elements V in Eq. (2.1) are no longer diagonal in spin space. Instead, each is multiplied by U_{ij}, a randomly chosen SU(2) matrix, which describes the spin rotation due to strong SO scatterers on each bond.[12,31] Equation (2.5) for the overlap of wave functions at the two end points must now include the initial and final spins, and the locator expansion now reads

$$\langle i\sigma|G(E)|f\sigma'\rangle = \sum_\Gamma\prod_{i_\Gamma}\frac{Ve^{iA}U}{E-\epsilon_{i_\Gamma}} . \tag{4.2}$$

Each bond along the path contributes a random spin rotation U, and a phase factor from the magnetic vector potential A. The NSS random energies $\epsilon_i=\pm W$ again simplify the energy denominators, and Eq. (2.6) for the sum of directed paths generalizes to

$$\mathcal{A} = \langle i\sigma|G(0)|f\sigma'\rangle = W(V/W)^t J(t) , \qquad J(t) = \sum_{\Gamma'}\prod_{i_{\Gamma'}}\eta_{i_{\Gamma'}}e^{iA}U . \tag{4.3}$$

After averaging over the initial spin, and summing over the final spin, the tunneling probability is

$$T=\tfrac{1}{2}\mathrm{Tr}(\mathcal{A}^{\dagger}\mathcal{A})=W^2(V/W)^{2t}I(t)\ ,$$
$$I(t)=\tfrac{1}{2}\mathrm{Tr}(J^{\dagger}J)\ . \tag{4.4}$$

We numerically studied the statistical properties of $I(t)$ using a transfer-matrix method to exactly calculate I up to $t=1000$ for over 2000 realizations of the random Hamiltonian. As in Sec. II A, we found that the distribution is broad (almost log-normal), and that the appropriate variable to consider is $\ln I(t)$. Variations of the mean $\langle \ln I(t)\rangle$ versus t are plotted in Fig. 16, with and without SO and at various magnetic fields.[36] In all cases, the asymptotic slope gives the change in the global contribution to the inverse localization length ξ_g^{-1}. The first set of curves in the bottom of Fig. 16 are results from the previous section, included for the sake of comparison. The larger slopes in higher magnetic fields indicate the increase in the localization length that saturates at the limiting value corresponding to the random-phase Hamiltonian. Turning on the SO interactions is accompanied by a significant increase in slope beyond this limit. However, in the presence of SO, addition of the magnetic field leads to no further increase in slope. In fact, there is a much smaller enhancement of tunneling that is not observable at the scale of the bottom figure. The MC with SO is thus plotted separately in the top part of Fig. 16. The curves appear to asymptotically approach a constant, indicating a t-independent MC, and no change in the localization length.

We also studied the scaling properties of the MC with SO by collapsing the data in Fig. 16. The appropriate scaling axis, as indicated in Fig. 17, is $Bt^{3/2}$, and the scaling function behaves as

$$\langle \ln I(t,B)-\ln I(t,0)\rangle=\begin{cases} cB^2t^3 & \text{if } B^2t^3<1 \\ C\approx 0.25 & \text{if } B^2t^3>1\ . \end{cases} \tag{4.5}$$

This is to be contrasted to the Bt^2 scaling of Fig. 11 in the absence of SO. The effected area in this case appears to be bounded by typical random walks.[27]

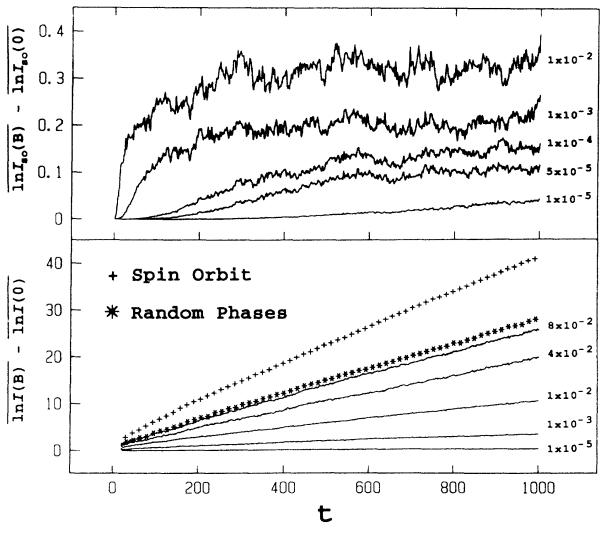

FIG. 16. Log-averaged tunneling probability vs t, with and without SO, and at various magnetic fields. Bottom: increase in tunneling (MC) *without* SO (solid lines) at fields indicated to the right. Saturated behavior in a strong magnetic field (*) is simulated by replacing the gauge potential with random phases on bonds. Addition of SO in zero field leads to the curve (+) labeled I_{SO}. Top: since MC *with* SO is small, the increase is plotted at enlarged scale.

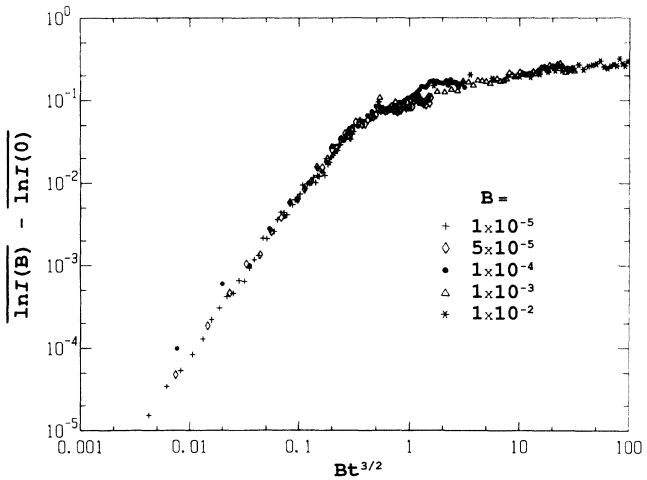

FIG. 17. Scaling of MC with B and t in the presence of SO, obtained by collapsing the data in the previous figure.

B. Analytical results

We can gain some analytic understanding of the distribution function for $I(t,B)$ by examining the moments $\langle I(t)^n\rangle$. From Eqs. (4.3) and Eq. (4.4) we see that each $I(t)=(1/2)\mathrm{Tr}(J^{\dagger}J)$ represents a forward path from i to f, and a time reversed path from f to i (see replica arguments in Sec. III). For $\langle I(t)^n\rangle$, we have to average over the contributions of n such pairs of paths. First, averaging over the random signs of the site energies forces a pairing of the $2n$ paths (since any site crossed by an odd number of paths leads to a zero contribution). Next, we must average over the random SO matrices on each bond. Again, a bond crossed only once gives zero average ($\langle U_{\alpha\beta}\rangle=0$). From the orthogonality relation for group representations,[58] we have

$$\int \Gamma^k(g)^*_{ij}\Gamma^{k'}(g)_{i'j'}W(\alpha_1,\ldots,\alpha_n)d\alpha_1,\ldots,d\alpha_n$$
$$=\frac{\delta_{ii'}\delta_{jj'}\delta_{kk'}}{\lambda_k}\int W(\alpha_1,\ldots,\alpha_n)d\alpha_1\cdots d\alpha_n\ , \tag{4.6}$$

where $\Gamma^k(g)_{ij}$ is the ij matrix element of a representation of the group element g, and $W(\alpha_1,\ldots,\alpha_n)$ is an appropriate weight function so that the matrix space is sampled uniformly as the continuous parameters $\alpha_1,\ldots,\alpha_n$ vary [e.g., Euler angles for a representation of SU(2)]. Finally, λ_k is the order of the representation k. Choosing the Euler angle parametrization of SU(2), it can be shown

that only the following paired averages are nonzero:

$$\langle U_{\alpha\beta}U^{*}_{\alpha\beta}\rangle=\tfrac{1}{2},\quad \langle U_{\uparrow\uparrow}U_{\downarrow\downarrow}\rangle=\tfrac{1}{2},\quad \langle U_{\uparrow\downarrow}U_{\downarrow\uparrow}\rangle=-\tfrac{1}{2}\ , \tag{4.7}$$

and their complex conjugates. Thus two classes of paired paths survive the averaging: (i) *Neutral paths,* in which one member is selected from J and the other from $J^{\dagger}$. Such paths are forced to have parallel spins and do not couple to the magnetic field. (ii) *Charged paths,* in which both elements are taken from J or from $J^{\dagger}$. Such pairs must have antiparallel spins and couple to the magnetic field, like particles of charge $\pm 2e$.

Since the factor of $\frac{1}{2}$ from the bond averages in Eq. (4.7) cancels with the choice of two spin directions at each site, $\langle I(t)\rangle$ still asymptotically scales as 2^t. To calculate higher moments $\langle I(t)^n\rangle$, we must first compute the exchange factors at each intersection. With SO, this involves also taking into account the allowed spin exchanges. Two neutral paths entering the interaction can have indices $(\alpha\alpha)$, $(\alpha\alpha)$ or $(\alpha\alpha),(\beta\beta)$; there are two possibilities for the first ($\alpha=\uparrow$ or $\downarrow$) and two for the second. In the former case, however, there are two exchanges preserving neutrality, while in the latter only one exchange is possible satisfying this constraint. Hence an overall multiplicity of $(2\times 2+2\times 1)\times(\frac{1}{2})^2=\frac{3}{2}$ is obtained, where the last factor comes from the averages in Eq. (4.7). Thus the intersection of two paired paths result in an exchange attraction of $\frac{3}{2}$; a signature of the symplectic symmetry. The sum over n attracting paths, as in Eq. (2.13), then leads to

$$\langle I(t)^n\rangle = A(n)2^{nt}\exp[\rho n(n^2-1)t]\ , \tag{4.8}$$

where we have also included an overall n-dependent amplitude as in Sec. III C. [We confirmed numerically that SO interactions do indeed belong to this universality by numerically checking the $\frac{1}{3}$ exponent for the growth of fluctuations in $\ln I(t)$ required by Eq. (2.15).]

We can now appreciate the trends in Fig. 16, as the slopes are indicative of the statistical attraction factors. Without SO, the magnetic field gradually reduces the attraction factor from 3 to 2, leading to the increase in slope. Addition of SO to the Hamiltonian has the similar effect of suddenly decreasing the attraction to $\frac{3}{2}$. Why does the addition of the magnetic field lead to no further change in ρ in the presence of SO? Without SO, the origin of the continuous change in the attraction factor is the type of exchange indicated in Fig. 6, whereby a charged bubble appears in the intersection of two neutral paths (see Sec. III). In the presence of SO, from the averages in Eq. (4.7) we find the contribution of such configurations to be zero: Such a generic bubble is depicted in Fig. 18. To produce intermediate charged paths (with their antiparallel spins), the entering pair must have indices of the type $(ii),(\bar{i}\bar{i})$ (where $\bar{\downarrow}=\uparrow$, and $\bar{\uparrow}=\downarrow$). Within the bubble we can have intermediate sites labeled $(j\bar{j})$ and $(k\bar{k})$, which must be summed over due to matrix contractions. It is easy to check that, independent of the choice of j, if the incoming and outgoing spins (i and m) are the same on a branch, it contributes a positive sign,

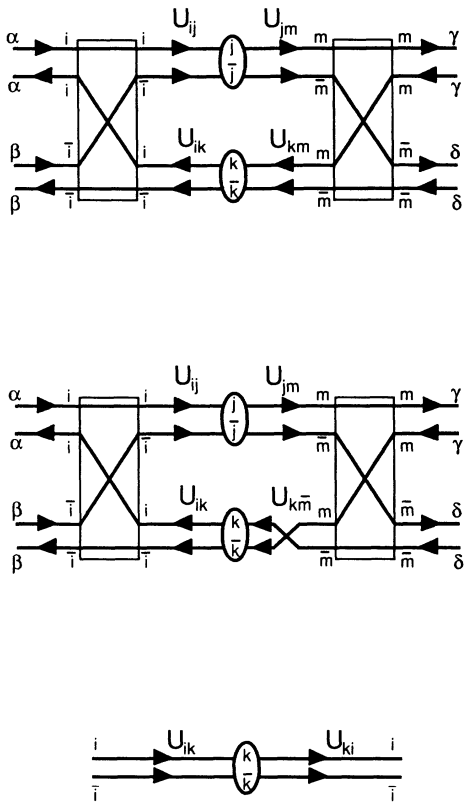

FIG. 18. Top: generic bubble diagram labeled with spin indices. Any choice of spins gives a positive contribution. Bottom: paths extending through the whole system are required to have the same initial and final indices due to the trace operation.

while if they are opposite the overall sign is negative. (Thus all possible sets of labels i, j, k, and m of Fig. 18 give a positive sign.) However, for any choice of i and m, one may choose similar (e.g., $i\rightarrow m$ on both branches), or opposite (e.g., $i\rightarrow m$ on top and $i\rightarrow\bar{m}$ on lower branch) connections. The difference in sign between the two choices thus cancels their overall contributions. Thus the neutral paths traverse the system without being affected by charged segments, and hence the magnetic field; their attraction factor stays at $\frac{3}{2}$, and $\rho=\xi_g^{-1}$ is unchanged.

The smaller positive MC observed in the simulations is due to changes in the amplitude $A(n)$ in Eq. (4.8). Unlike the random-phase Hamiltonian, considered in Sec. III C, charged paths do contribute to the tunneling. In fact, the operation of the trace in Eq. (4.4) insures a positive contribution, as indicated in Fig. 18. However, due to their lack of interactions, we may treat the charged and neutral paths as independent. At zero field, any of the pairings into charged and neutral paths is acceptable, while at finite fields only neutral pairs survive. As discussed in Sec. III C, this leads to a reduction in the amplitude $A(n)$ for $n\geq 2$, but an increase in $\ln I$ (a positive MC). The typical value of $\ln I$ thus increases by a t-independent amount. This behavior is similar to the predictions of the IPA, and is indeed due to the independence of charged and neutral paths. Since according to Eq. (3.5) the typical scale of decay for charged paths de-

pends on the combination $Bt^{3/2}$, we can explain the scaling obtained numerically in Fig. 17.

It is conceptually interesting to generalize the problem to higher "spins," using SU(n) random matrices in Eq. (4.1). All the relevant averages in replica space now involve direct products of two SU(n) matrices. For neutral paths, we can compute all the direct products of the form $U_{ij}U_{kl}^{*}$ as before, using the orthogonality relations in Eq. (4.6), and

$$\langle U_{ij}U_{kl}^{*}\rangle=\frac{\delta_{ik}\delta_{jl}}{n} . \tag{4.9}$$

For the "charged" averages of the form $U_{ij}U_{kl}$, we resort to the Clebsch-Gordan (CG) decomposition in order to write these products as a sum of irreducible representations of SU(n). This decomposition is very well known and it has the general form[58]

$$n\otimes n=\frac{n(n+1)}{2}\oplus\overline{\frac{n(n-1)}{2}} . \tag{4.10}$$

For $n=2$ this relation yields the decomposition $3\oplus 1$, i.e., the familiar triplet and the singlet states. As can be seen from the general formula, no other direct product of the above form yields the identity representation except $n=2$. The identity yields the only nonzero contribution when the average is performed, so that the only group in which charged paths survive is SU(2). No other continuous group exhibits an MC. This trivially includes the case of random phases, i.e., the group U(1), since

$$U^{\alpha}\otimes U^{\beta}=U^{\alpha+\beta} , \tag{4.11}$$

where α and β label the representation of the form $U^{\alpha}=\exp(i\alpha\theta)$. For $\alpha,\beta>0$ the trivial direct product for charged paths does not yield the identity in the CG expansion, and thus there is no MC with U(1) impurities present.

The exchange attraction between neutral paths can also be computed for SU(n) impurities, and equals

$$\alpha=\frac{n+1}{n} . \tag{4.12}$$

This reproduces 2 for $U(1)$ or random phases, and $\frac{3}{2}$ for SU(2) or SO scattering. The attraction vanishes in the $n\to\infty$ limit, which must then correspond to the IPA approximation. We thus find that the statistical exchange factors are universal numbers, simply related to the symmetries of the underlying Hamiltonian. The attractions in turn are responsible for the formation of bound states in replica space, and the universal scaling of the moments in Eq. (4.8). Although the parameter $\rho=\xi_g^{-1}$ reflects the variations in the exchange attraction, it is not by itself universal, but model dependent. In fact, since the single parameter ρ completely characterizes the distribution, the variations in the mean and variance of the NSS model should be perfectly correlated. This can be tested numerically by examining, respectively, coefficients of the mean and the variance from Eq. (2.15) for the different cases studied. The results plotted in Fig. 19 do indeed fall on a single line, parametrized by ρ. The largest value corresponds to the NSS model for $B=0$ and no SO (orthogonal symmetry, exchange attraction 3). Introduction of a field gradually reduces ρ until saturated at the limit of random phases (unitary symmetry, exchange attraction 2). SO scattering reduces ρ further (symplectic symmetry, exchange attraction $\frac{3}{2}$). The final point corresponds to independent paths with $\rho=0$. An interesting observation based on Fig. 19 is that the *relative attractions* for the three symmetries are $(\frac{3}{2}-1):(2-1):(3-1)=1:2:4$. If the bound-state energy $\rho=\xi_g^{-1}$ were simply proportional to the attraction, we would conclude the ratios 1:2:4 for the global localization lengths ξ_g^{-1} at these points. These are precisely the ratios predicted by the RMA.[32] Unfortunately at least for the NSS model, ρ is a nonlinear function of this relative attraction. The projected ratios along the horizontal axis in Fig. 19 for ξ_g^{-1} are approximately 1:2.2:5.7.

C. Comparison with other work

The independent-path approach has been recently extended by Meir *et al.*[31] to include SO effects. While the predictions of IPA are in contradiction with our results in the absence of SO, for reasons explained in the previous section, they are close to the mark when the SO interactions are turned on. Meir *et al.* predict a universal increase of $C=\frac{5}{6}-\ln 2\sim 0.14$ in $\langle \ln I\rangle$ for sufficiently strong fields. The numerical results in Fig. 17 actually give a saturation value $C\simeq 0.25$. However, we believe that this increase is nonuniversal, as the limiting value changed upon reducing the concentration of SO impurities.

The *random-matrix approach* (RMA) takes as its input only the symmetries of the transfer matrix M of an N-channel elastic-scattering system. The two-probe Landauer formula[59] is then used to relate the conductance g to the eigenvalues of the matrix $X=[(M^{+}M)+(M^{+}M)^{-1}-2I]/4$ via

$$g=2\sum_{a=1}^{N}\left[\frac{1}{1+\lambda_a}\right] . \tag{4.13}$$

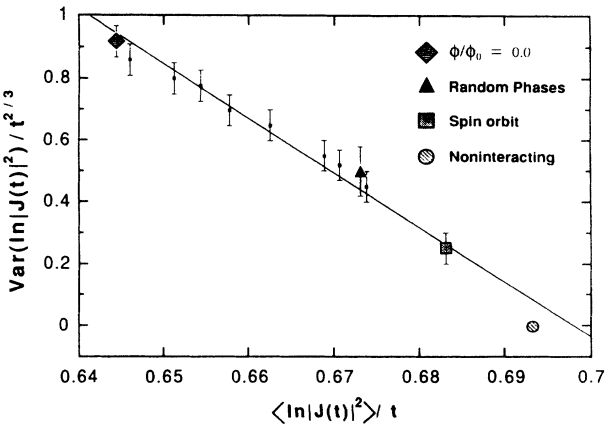

FIG. 19. Complete hierarchy of the exchange attractions between paired paths, reflecting the various Hamiltonian symmetries. Diamond, orthogonal case; triangle, the unitary limit; square, symplectic case; circle, the noninteracting limit corresponding to the IPA, and also to SU(n) with $n\to\infty$. Small squares correspond to finite magnetic fields but no SO.

The distribution for g is then obtained from the joint probability distribution of eigenvalues $P(\{\lambda_a\})$. There is also an underlying assumption of a single-parameter scaling, which is strongly supported only in the weakly localized regime. Recent work by Pichard *et al.*[32] extends the RMA to the strongly localized regime. It predicts[32] that the magnetic field results in a doubling of the localization length ξ in the absence of SO, and a halving of ξ with SO, in clear contradiction to our results. The RMA approach includes both forward-scattering and backscattering paths, yet despite its simplicity and generality, it suffers from a number of shortcomings. First, it is assumed at the outset that a single parameter is sufficient for characterizing the problem. However, Eq. (2.16) demonstrates that, in the strongly localized regime, the localization length (obtained from the tunneling probability) involves both a global and a local factor. Hence variations in ξ cannot be universal. Second, by considering the most general random matrices, the approach loses all information on spacial connectivity and dimensionality. (All channels are treated equivalently.[60]) The equivalent approximation for spin problems allows any spin in one layer to interact with *all* spins in neighboring layers. Thus it has the flavors of both one-dimensional and infinite-range models. (Using heuristic arguments, Bouchaud[33] also concludes that a factor-of-2 increase in ξ is only valid for quasi-one-dimensional systems.) The correct approach is to consider the ensemble of sparse random matrices in which only elements close to the diagonal are nonzero[61] (see also Ref. 60). Finally, we note there is no change in ξ with SO. The latter is due to the form of the Hamiltonian that excludes Zeeman-splitting terms. Such terms are certainly allowed by symmetry, but involve a much higher energy cost. The RMA cannot account for such subtleties.

We know of only three experimental measurements of SO effects on materials exhibiting VRH,[57,32,28] and they present conflicting results. The work by Shapir and Ovadyahu[57] was done on In_2O_{3-x} films doped with Au, a heavy element giving rise to SO scattering in the samples. These samples exhibit well-defined two-dimensional VRH behavior ($\sigma=\sigma_0\exp[-(T_0/T)^{1/3}]$ from Eq. (1.2)) and can be prepared to have widely varying conductances so that they are at a "controlled distance" from the metal-insulator transition. Samples with resistance less than 1 MΩ exhibit a behavior similar to metallic samples, i.e., a regime of negative MC, changing to positive MC at a well-defined field H^*. This is attributed[57] to an interplay between weak-localization effects (causing negative MC with SO) at scales less than ξ, and strong-localization effects (positive MC) at scales larger than ξ. The samples with higher resistivity, on the other hand, are surprisingly insensitive to the presence of SO, showing only a positive MC, virtually indistinguishable from undoped samples with similar zero-field resistivity. It is worth noting that positive MC effects are seen for the samples where the ratio t/ξ is the largest (from $t/\xi\sim 6$ to 14), while metalliclike effects are seen when $t/\xi\sim 1$. This is also evident in another experimental system discussed below.

The insensitivity to SO is certainly in conflict with results of Fig. 16 at high concentrations of such impurities. Actually, Shklovskii and Spivak[18] have recently suggested such insensitivity in the directed-path approximation. They maintain that the scattering matrix element, $U\propto(1-i\epsilon k\times k'\cdot\sigma)$, is particularly small in forward scattering, since k and k' are almost parallel. Although even such small random rotations should asymptotically produce the same behavior, due to long crossover effects, a more-dilute SO concentration may well reproduce the experimental findings of Ref. 57. We do note, however, that the sign of MC at small fields and low temperatures cannot be changed by such microscopic details. The microscopic details can only modify the local contribution to $\langle \ln T\rangle$ in Eq. (4.4). Such local factors must be analytic in B, and hence their contribution to MC scales as B^2t. Meanwhile, the global contributions scale as B^2t^3 [from Eq. (4.5)] with SO, or as $B^{1/2}t$ without [from Eq. (3.7)]. Therefore, there is always a positive MC at low fields at sufficiently large t (it may cross over to a negative MC at higher fields). Numerical simulations[31] at the scale of ξ are in agreement with such a picture. A positive MC in the localized regime can only be reconciled with the negative MC, predicted by the weak-localization theories with strong SO, through a possible phase transition.[62] It is possible that the observed change of sign in the experiments[57] is a finite-temperature manifestation of such a zero-temperature phase transition. It would be very interesting to clarify this possibility by further theoretical and experimental studies.

The other experimental work is from the Saclay group of Pichard, Sanquer, Slevin, and Debray[32] and more recently Hernandez and Sanquer.[28] In the first work they study both samples with (amorphous Y_xSi_{1-x} alloy) and without (GaAs/Si doping) SO scattering which exhibit three-dimensional Mott hopping behavior. They are interested in observing changes between (a) orthogonal and unitary Hamiltonians by submitting GaAs to a strong magnetic field, and (b) symplectic and unitary systems by again applying the field to Y_xSi_{1-x}. In case (a) random-matrix theory predicts a positive MC due to a doubling of the localization length, while for (b) it predicts a large negative MC due to the halving of ξ. [They extract ξ from the characteristic temperature, $T_0\sim 1/n(E_f)\xi^3$ in Eq. (1.2)]. They obtain results in qualitative agreement with the RMA. However, especially in light of the findings of Shapir and Ovadyahu,[57] it not clear how far the Y_xSi_{1-x} system is from the metal-insulator transition. In this work, the estimated hopping length t is of the same size as the localization length ξ, making weak-localization effects quite important (see discussion in the Introduction). On the other hand, the "distance" from the metal-insulator transition is a central issue in the work by Hernandez and Sanquer,[28] where a careful experimental study was conducted with Y_xSi_{1-x} samples exhibiting various t/ξ ratios. Different regimes are found; a weak insulating range ($t/\xi\sim 1$), close to the transition, where weak-localization effects are apparent and thus a negative MC is found, and the strong-localization limit ($t/\xi\gg 1$), where a positive MC is measured as predicted by the directed-path approach. As discussed in the Introduction, higher t/ξ ratios correspond more closely to the domain of validity of the ap-

proximations used in this work. In view of the fact that weak-localization effects are observed in the less strongly insulating samples, it is possible that the RMA treatment is indeed more appropriate to this regime. Further theoretical and experimental work is necessary to provide a more coherent and unified picture of the rich variety of MC behaviors occurring in disordered insulators.

V. THE PROBABILITY DISTRIBUTION FOR TUNNELING

A. Nonuniversality of high moments

The issue of how many parameters govern the scaling theory of localization is still a controversial topic even ten years after the introduction of the one-parameter scaling hypothesis.[3] The situation seems clear for metallic systems of dimensionality $d>2$, far from the localization transition. In this regime, single-parameter scaling seems to hold, as shown by a number of approaches.[39,63,64] However, the nature of the distribution function for the conductance changes quite dramatically on approaching the localization transition, and for the insulating state. We first briefly review some interesting work by Altshuler, Kravtsov, and Lerner (AKL) (Ref. 39) and Shapiro[63] pertaining to this issue. To study the conductance probability distribution, AKL computed its moments in the framework of an extended nonlinear σ model.[39] In the weakly localized regime, they find a probability distribution that is close to a Gaussian except for long log-normal tails. These long tails carry information about high nonuniversal cumulants and disappear in the limit $L \gg \xi$, where L is the sample size. In this case, the nonuniversal tails are associated with finite-size effects, and the limiting distribution is described by a single parameter. On the other hand, at the transition in $2+\epsilon$ dimensions, these tails cause sufficiently large moments to diverge in L; i.e., nonuniversal features remain in the large-L limit. AKL conjecture a log-normal distribution on the insulating side, although the analytical results cannot be extended to this regime. Shapiro[65] has pointed out that the nonuniversality of the moments is not inconsistent with a universal conductance distribution at the transition, and proposes such a distribution that reproduces the moments of AKL. The key is that, for distributions with power-law tails large enough, moments are divergent. (Conversely, if the nth moment increases faster than $n!$, the probability distribution cannot be uniquely inferred.[66])

On the basis of simple arguments, and a Migdal-Kadanoff rescaling approximation, Shapiro[63] and Cohen, Roth, and Shapiro[64] confirm the validity of single-parameter scaling in the weak-disorder regime, but find a two-parameter scaling[64] for strongly localized electrons. They note that such behavior emerges quite naturally for one-dimensional systems in which the conductance g is log-normally distributed. Except in the weak-scattering limit, the mean and variance of lng are independent, giving the two parameters of the theory. The results of the previous chapters are in qualitative agreement with such two-parameter scaling. The computation of the localization length based on the tunneling amplitude involves both a *local* factor $\xi_0^{-1}=2[\ln(\sqrt{2}W/V)]$ and a *global* factor $\xi_g^{-1}=\rho$. The former is the main contribution to the decay of the wave function, while the latter also controls the fluctuations. In fact, according to Eq. (4.8), ρ completely controls the asymptotic behavior of the moments, and hence the distribution function. Indeed, numerical simulations confirm the universal nature of the distribution in the sense that the scaling of the fluctuations is not changed by introducing a field, turning on SO interaction, or changing the concentration of the impurities.

We note, however, that Eq. (4.8) cannot be valid for large moments. Since $J(t)$ is bounded by 2^t (from a uniform configuration with positive site energies), we must have $\langle |J|^{2n} \rangle < 2^{2nt}$. Therefore, at large n, the exponent in Eq. (4.8) must increase at most linearly in n, and not as n^3. [Using $\rho \approx 0.053$ indicates that deviations from Eq. (4.8) must already appear for $n \approx 4$.] The breakdown of this equation can again be traced to the nonuniversality of the high moments, as illustrated by the following argument. Equations (4.8) and (2.13) are obtained from a *continuum description* of the problem in Eq. (2.10). To understand the origin of the n^3 dependence, we resort to the following scaling argument, valid for large n. We can estimate the size R of the bound state of the Hamiltonian by estimating the energy of n particles confined to a size R as

$$\epsilon_n = \frac{\gamma n}{R^2} + \frac{\sigma^2 n^2}{4R} \ . \tag{5.1}$$

Minimizing this expression with respect to R gives $R \propto l^*/n$ and $\epsilon_n \propto n^3/\xi_g$ [$l^* \propto \gamma/\sigma^2 \propto (\gamma \xi_g)^{1/2}$]. Thus, as n increases, the particles become more tightly bound, and eventually the continuum approximation breaks down when R approaches the lattice spacing. (Using $\xi_g \approx 20$, we again estimate that this collapse occurs for $n \approx 4$ in the NSS model.) In this limit, the n replicas follow the same trajectory and hence feel the corresponding moment of the local distribution chosen for the bonds. This clearly leads to a nonuniversality of the high moments that does not go away as the size t is increased. Thus size-dependent tails calculated by AKL for moments of g at the transition are similarly present for the tunneling probability of localized electrons.

Does the breakdown of continuum description for $n \approx l^*$ invalidate the scaling of cumulants predicted in Eq. (2.15)? (After all, the $\frac{1}{3}$ exponent for fluctuations is numerically verified.) The answer is the identification of cumulants from Eq. (2.14) relies on *an expansion around* $n \to 0$. Although it is hard to visualize such a limit of an n-particle system, mathematically the continuum limit should work well as $n \to 0$, since $R \propto l^*/n \to \infty$. In general, for the problem on the lattice, the ground-state energy ϵ_n is a complicated function of n. However, we expect $\lim_{n\to 0}\epsilon_n = \rho n(n^2-1)$; while $\lim_{n\to\infty}\epsilon_n = C_0(n)$, where $C_0(n)$ is related to the nth moment of the local impurity distribution. [For the NSS model $C_0(n) \to n \ln 2$.] Pre-

dictably, the behavior of large moments is almost completely determined by those very rare configurations that allow maximum tunneling (with lowest impurity). Since the tunneling probability is exponentially dependent on the length t, the t dependence is a natural part of the scaling of the moments (unlike the metallic case, where it vanishes in the large-size limit). Going back to Fig. 8, the mean and fluctuations of the distribution are correctly described by Eqs. (2.15), while the tails are nonuniversal, and model dependent, even in the large-t limit. Replica treatments that only focus on the large-n behavior of moments[45] may well lead to incorrect conclusions.

We recently verified the nonuniversality of high moments for the related problem of directed polymers,[43] for which the random signs $\eta_i = \pm$ in Eq. (2.6) are replaced by positive random weights w_i. A position-space RG scheme, exact on a hierarchical lattice, developed by Derrida and Griffiths[67] was used to follow the scaling of the overall sum over directed paths. On these lattices, the problem is reduced to determining the stable laws for combining random variables in a nonlinear way. We focused on the evolution of the characteristic function $f(n) \equiv \ln\langle w^n \rangle$. Details of the procedure are left for future publications, and only the pertinent results are summarized here. We find that after sufficient iteration, the distribution converges to a stable limit. For small n, the limiting behavior of $f(n)$ is independent of the initial random distribution, while for large n it is completely determined by the initial $f_0(n)$. A typical set of results is presented in Fig. 20.

B. Higher dimensions

All of the discussion so far has centered on two-dimensional systems. In this section we address what happens in other dimensions d. Actually, the simplest example of a one-dimensional system already qualitatively exhibits most of the features found in $d=2$. Consider a strip of width w and length t. For $\omega \approx t$, the two-dimensional behavior should be recovered, while $t \gg w$ corresponds effectively to $d=1$. We simulated the NSS model on such strips to investigate the crossover between $d=2$ and 1 behavior. Summation of forward-scattering paths again leads to wide distributions that are approximately log-normal, with $\langle \ln|J(w,t)| \rangle$ increasing as t. However, as indicated in Fig. 21, the variance of $\ln|J(w,t)|$ depends on w/t. Wide strips ($w=400$, and for $t \leq 1000$) show the scaling $t^{1/3}$, characteristic of two dimensions, while narrow strips at sufficiently large t exhibit a variance proportional to t. The one-dimensional behavior is quite easy to interpret: the strip can be subdivided into roughly t/w segments of width w, each with a tunneling amplitude A_i (the multiplicity of channels does not substantially modify the argument). The overall amplitude for tunneling is $J \approx \prod_i A_i$. Clearly, $\ln|J|^2 = \sum_i \ln|A_i|^2$, and since the A_i are independent for different segments, the central-limit theorem can be used to deduce that $\ln|J|^2$ is Gaussian distributed, with mean and variance scaling as t in agreement with Fig. 21.

The above calculation of the tunneling probability based on the summation of forward-scattering paths suggests that the mean and variance of $\ln|J|^2$, although proportional, may have different amplitudes. Thus two parameters are necessary to specify the probability distribution. However, the conductivity of the one-dimensional Anderson chain can be calculated fully *without the forward-scattering approximation.*[68] This approach also gives an approximately log-normal distribution for the resistivity, but the mean and variance of the distribution are correlated, i.e., the distribution can be specified by one parameter. The random-matrix approach[12,60,69] is quite suited to quasi-one-dimensional systems and also gives a one-parameter distribution. However, Cohen, Roth, and Shapiro[64] have emphasized that in both cases this conclusion arises from a weak-disorder assumption, and that two parameters are necessary to describe the strong-disorder limit. It is precisely in this limit that the approximation to forward-scattering paths is expected to

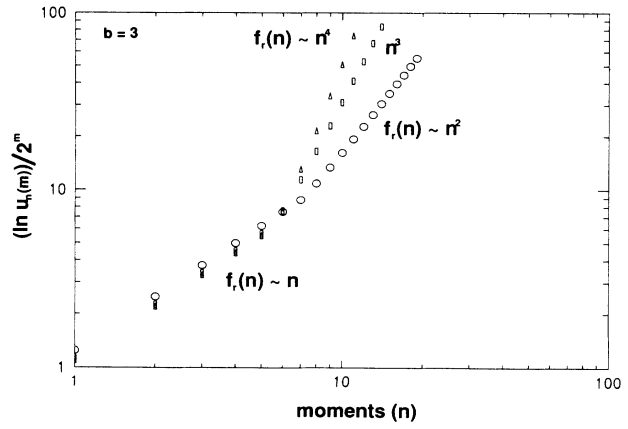

FIG. 20. Stable moment dependences generated from three different initial distributions of randomness: circles, $f_0(n)=0.15n^2$; squares, $f_0(n)=0.03n^3$; triangles, $f_0(n)=0.005n^4$. The renormalized $f(n)$ starts out with a linear dependence, and then crosses over to the same form as $f_0(n)$.

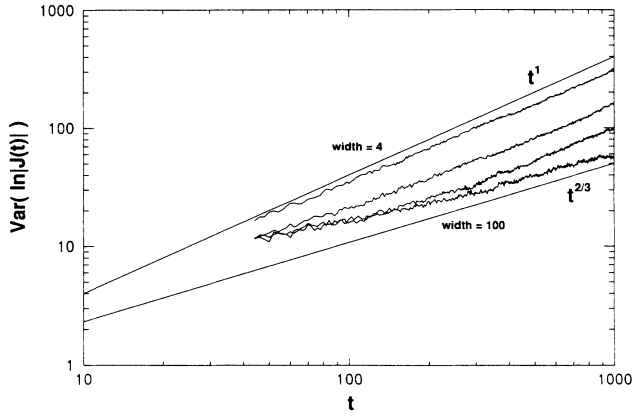

FIG. 21. Numerical calculation of the NSS model on strips. As the strip width is increased from four lattice spacings to 100, scaling of fluctuations in $\ln|J|$ makes a crossover from the $d=1$ exponent $\omega=\frac{1}{2}$ to the $d=2$ exponent of $\omega=\frac{1}{3}$. (The intermediate strips have widths 10 and 20.)

be valid. Finally, the addition of a magnetic field or SO scattering to the strips is expected to lead to changes in the tunneling probability. We did not pursue this direction, but note that again in the forward-scattering approximation the changes in the localization length will not be universal. This is again at variance with the RMA predictions of doubling or halving of ξ. It would certainly be interesting to find out to what extent the predictions of the RMA can be extended to the strong-scattering limit. Studies of simple one-dimensional systems may thus provide a bridge between these two approaches.

For the two-parameter log-normal distribution in $d=1$, the moments scale as

$$\langle |J(t)|^{2n}\rangle = A(n)\langle |J(t)|\rangle^{2n}\exp[\rho n(n-1)t] , \qquad (5.2)$$

qualitatively similar to Eq. (4.8). The nonuniversality of high moments is also present in $d=1$: It is well known that the characteristic function for the sum of t-independent random variables is t times the characteristic function for one variable. The terms in Eq. (5.2) are just the first two terms in an expansion of the characteristic function in powers of n. Again, the behavior at very large n (for fixed t) is completely determined by the large moments of individual random variables; physically, these moments are dominated by exceptionally "good" realizations.

The replica (moment) analysis of Sec. II C can be extended to higher dimensions d: In calculating $\langle (J^*J)^n\rangle$, the averaging over the $\pm$ potential disorder pairs up the paths. The n paired paths are subject to precisely the same exchange attraction factors for intersection calculated earlier—3 for orthogonal, 2 for unitary, and $\frac{3}{2}$ for symplectic Hamiltonian symmetry. These attracting paths can be regarded as world lines of n particles in $d'=d-1$ dimensions. Calculating $\langle (J^*J)^n\rangle = \exp(-\epsilon_n t)$ now reduces to finding the ground-state energy of n particles with a short-range attraction. [In particular, in order to identify the cumulants through the small-n expansion of Eq. (2.14), the form of ϵ_n must be extendable to $n\to 0$.] Unfortunately, the ground-state is only known exactly in $d'=1$. However, it is possible to draw a number of important conclusions for higher d'. It is known that in $d'\le 2$ any attractive potential will always lead to formation of a bound state. This implies that in three dimensions the localization length [ξ defined through Eq. (2.16)] has both a local and a global contribution. Again, the introduction of a magnetic field should lead to a nonuniversal increase in ξ in the absence of SO. With SO, there will be a smaller positive MC, but no change in ξ. Presumably, the scaling forms of previous chapters are still applicable to $d=3$. To specify the distribution function for $\ln|J(t)|$ completely, we also need the dependence of its fluctuations on t. In the absence of the correct energy, we can make no exact statements about this dependence. However, the analogy to the problem of directed polymers[43] mentioned earlier allows us to take advantage of the large body of numerical work on this, and a related interface growth, problem.[70] The numerical studies in $d=3$ suggest fluctuations in $\ln|J(t)|$ scaling as t^{ω}, with $\omega\approx 0.2$–0.25.[71,72] Figure 22 shows some preliminary numerical results for the NSS model in $d=3$ for system sizes of $300\times 300\times 300$. The observed exponent, $\omega\approx\frac{1}{5}$, is close to the lower values in this range.

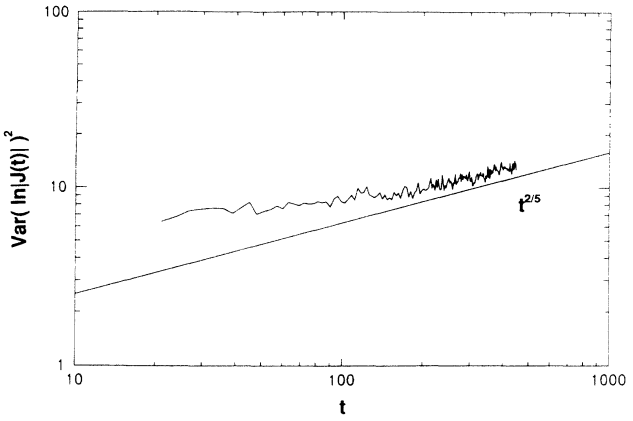

FIG. 22. Preliminary data for the three-dimensional NSS model showing convergence to an exponent of $\omega\approx\frac{1}{5}$.

Three is a critical dimension of the theory in that for $d>3$ the strongly localized regime can exhibit a phase transition between two distinct behaviors. This follows from above the mapping to attracting quantum particles: For $d'>2$, a critical amount of attraction is necessary to form a bound state. The phase in which the particles do form a bound state has properties similar to those described in $d=2$ and 3. Current numerical estimates,[72] based on the analogy to directed polymers,[70] suggest fluctuations in $\ln|J(t)|$ growing as $t^{1/d+1}$. This is consistent with generalizing the small-n-moment behaviors in Eqs. (5.2) and (4.8) to

$$\langle |J(t)|^{2n}\rangle = A(n)\langle |J(t)|\rangle^{2n}\exp[\rho n(n^d-1)t] . \qquad (5.3)$$

The applicability of this suggestive form certainly requires further analysis. For $d>3$, there is also a new phase in which the particles do not form a bound state. In this case the intersections between paths are asymptotically irrelevant, and hence the assumptions of the independent-path approach[27,30,31] are justified. The probability distribution for tunneling in this case is indeed a sharp Gaussian (the variance of J grows exponentially with the number of paths). One can imagine a transition between the two phases upon changing impurity scattering, or by a magnetic field. In particular, the effective line tension for the paths is connected to ξ^{-1}, and is expected to vanish at the localization transition. A smaller line tension actually favors the formation of the bound state. Thus the most likely scenario is that, immediately after the localizing transition, the system shows anomalous fluctuations described by Eq. (5.3), and shows the type of response to magnetic fields and SO described earlier. Upon further localization, it may then make a transition to the type of phase correctly describable by IPA. As noted in the Introduction, the general arguments of this section should be equally applicable to describing the disordered phase of spin glasses and magnets with impurities.

ACKNOWLEDGMENTS

This work originated in a collaboration with Y. Shapir and X.-R. Wang, whose continuing advice has been invaluable. EM is fully supported by INTEVEP, Venezuela. The advice of B. Altshuler and P. Lee is greatly appreciated. We have also benefited from discussions with Y. Meir, N. Read, and N. Wingreen. MK is supported by the NSF through Grant No. DMR-90-01519, and the PYI program.

[1]P. W. Anderson, Phys. Rev. **109**, 1492 (1958).
[2]D. J. Thouless, Phys. Rep. **13**, 93 (1974); Phys. Rev. Lett. **39**, 1167 (1977).
[3]E. Abrahams, P. W. Anderson, D. C. Licciardello, and T. V. Ramakrishnan, Phys. Rev. Lett. **42**, 673 (1979).
[4]L. P. Gor'kov, A. I. Larkin, and D. E. Khmel'nitskii, Pis'ma Zh. Eksp. Teor. Fiz. **30**, 248 (1979) [JETP Lett. **30**, 248 (1979)].
[5]F. J. Wegner, Z. Phys. B **35**, 207 (1979).
[6]P. A. Lee and T. V. Ramakrishnan, Rev. Mod. Phys. **57**, 287 (1985).
[7]B. L. Altshuler, Pis'ma Zh. Eksp. Teor. Fiz. **42**, 530 (1985) [JEPT Lett. **41**, 648 (1985)].
[8]P. A. Lee and A. D. Stone Phys. Rev. Lett. **55**, 1622 (1985).
[9]B. L. Altshuler and B. I. Shklovskii, Zh. Eksp. Teor. Fiz. **91**, 220 (1986) [Sov. Phys.—JETP **64**, 127 (1986)].
[10]P. A. Lee, A. D. Stone, and H. Fukuyama, Phys. Rev. B **35**, 1039 (1987).
[11]G. Bergmann, Phys. Rep. **107**, 1 (1984).
[12]N. Zannon and J. L. Pichard, J. Phys. (France) **49**, 907 (1988).
[13]R. A. Webb and S. Washburn, Phys. Today **41** (12), 46 (1988).
[14]P. A. Lee and B. L. Altshuler, Phys. Today **41** (12), 36 (1988).
[15]N. F. Mott, J. Non-Cryst. Solids **1**, 1 (1968).
[16]A. Miller and E. Abrahams, Phys. Rev. **120**, 745 (1990).
[17]V. Ambegaokar, B. I. Halperin, and J. S. Langer, Phys. Rev. B **4**, 2612 (1971).
[18]B. I. Shklovskii and B. Z. Spivak, in *Hopping Conduction in Semiconductors,* edited by M. Pollak and B. I. Shklovskii (North-Holland, Amsterdam, 1990).
[19]B. I. Shklovskii and A. L. Efros, *Electronic Properties of Doped Semiconductors* (Springer-Verlag, Berlin, 1984).
[20]A. O. Orlov and A. K. Savchenkov, Pis'ma Zh. Eksp. Teor. Fiz. **44**, 34 (1986) [JETP Lett. **44**, 41 (1986)]; **43**, 421 (1986) [**43**, 540 (1986)].
[21]E. I. Laiko, A. O. Orlov, A. K. Savchenkov, E. A. Il'ichev, and E. A. Poltoratskii Zh. Eksp. Teor. Fiz. **93**, 2204 (1987) [Sov. Phys.—JETP **66**, 1258 (1987)].
[22]Z. Ovadyahu, J. Phys. C **19**, 5187 (1986).
[23]O. Faran and Z. Ovadyahu, Phys. Rev. B **38**, 5457 (1988).
[24]A. B. Fowler, IBM J. Res. Dev. **32**, 372 (1988).
[25]Ya. B. Poyarkov, V. Ya Kontarev, I. P. Krylov, and Yu. V. Sharvin, Pis'ma Zh. Eksp. Teor. Fiz. **44**, 291 (1986) [JETP Lett. **44**, 372 (1986)].
[26]F. P. Milliken and Z. Ovadyahu, Phys. Rev. Lett. **65**, 911 (1990).
[27]V. L. Nguyen, B. Z. Spivak, and B. I. Shklovskii, Pis'ma Zh. Eksp. Teor. Fiz. **41**, 35 (1985) [JETP Lett. **41**, 42 (1986)]; Zh. Eksp. Teor. Fiz. **89**, 11 (1985) [Sov. Phys.—JETP **62**, 1021 (1985)].
[28]P. Hernandez and M. Sanquer, Phys. Rev. Lett. **68**, 1402 (1992).
[29]H. L. Zhao, B. Z. Spivak, M. P. Gelfand, and S. Feng, Phys. Rev. B **44**, 10 760 (1991).
[30]U. Sivan, O. Entin-Wohlman, and Y. Imry, Phys. Rev. Lett. **60**, 1566 (1988); O. Entin-Wohlman, Y. Imry, and U. Sivan, Phys. Rev. B **40**, 8342 (1988).
[31]Y. Meir, N. S. Wingreen, O. Entin-Wohlman, and B. L. Altshuler, Phys. Rev. Lett. **66**, 1517 (1991).
[32]J. L. Pichard, M. Sanquer, K. Slevin, and P. Debray, Phys. Rev. Lett. **65**, 1812 (1990).
[33]J. P. Bouchaud (unpublished).
[34]E. Medina, M. Kardar, Y. Shapir, and X. R. Wang, Phys. Rev. Lett. **62**, 941 (1989).
[35]E. Medina, M. Kardar, Y. Shapir, and X. R. Wang, Phys. Rev. Lett. **64**, 1816 (1990).
[36]E. Medina and M. Kardar, Phys. Rev. Lett. **66**, 3187 (1991).
[37]See, e.g., A. M. Polyakov, *Gauge Fields and Strings* (Hardwood Academic, Chur, 1987).
[38]D. R. Hofstadter, Phys. Rev. B **14**, 2239 (1976).
[39]B. L. Altshuler, V. E. Kravtsov, and I. V. Lerner, Pis'ma, Zh. Eksp. Teor. Fiz. **43**, 342 (1986) [JETP Lett. **43**, 441 (1986)]; Zh. Eksp. Teor. Fiz. **91**, 2276 (1986) [Sov. Phys.—JETP **64**, 1352 (1986)].
[40]K. Gottfried, *Quantum Mechanics* (Addison-Wesley, Reading, MA, 1990).
[41]I. M. Lifshits and V. Ya. Kirpichenko, Pis'ma Zh. Eksp. Teor. Fiz. **77**, 989 (1979) [Sov. Phys.—JETP **50**, 499 (1979)].
[42]W. H. Press, B. P. Flannery, S. A. Teukolsky, and W. T. Vetterling, *Numerical Recipes* (Cambridge University, Cambridge, 1986).
[43]M. Kardar and Y.-C. Zhang, Phys. Rev. Lett. **58**, 2087 (1987).
[44]D. A. Huse and C. L. Henley, Phys. Rev. Lett. **54**, 2708 (1985).
[45]Y.-C. Zhang, Phys. Rev. Lett. **62**, 979 (1989); Europhys. Lett. **9**, 113 (1989); J. Stat. Phys. **57**, 1123 (1989).
[46]M. P. Gelfand, Physica A **177**, 67 (1991).
[47]M. Kardar, Nucl. Phys. B **290**, 582 (1987).
[48]J. P. Bouchaud and H. Orland, J. Stat. Phys. **61**, 877 (1990).
[49]Y. Shapir and X. R. Wang, Europhys. Lett. **4**, 1165 (1987).
[50]X. R. Wang, Y. Shapir, E. Medina, and M. Kardar, Phys. Rev. B **42**, 4559 (1990).
[51]X. C. Xie and S. DasSarma, Phys. Rev. B **36**, 9326 (1987).
[52]S. Obukhov, in *Hopping Conduction in Semiconductors* (Ref. 18), p. 338.
[53]M. Ya. Azbel, Zh. Eksp. Theor. Fiz. **46**, 929 (1964).
[54]B. I. Shklovskii and A. L. Efros, Pis'ma Zh. Eksp. Teor. Fiz. **84**, 811 (1983) [Sov. Phys.—JETP **57**, 470 (1983)].
[55]J. P. Bouchaud and H. Orland, J. Stat. Phys. **61**, 877 (1990).
[56]J. Krug and P. Meakin, J. Phys. A **23**, L987 (1990).
[57]Y. Shapir and Z. Ovadyahu, Phys. Rev. B **40**, 12 441 (1989).
[58]H. F. Jones, *Groups, Representations and Physics* (Hilger, Bristol, 1990).
[59]R. Landauer, Philos. Mag. **21**, 863 (1970).
[60]P. A. Mello and S. Tomsovic, Phys. Rev. Lett. **67**, 342 (1991).
[61]J. Cook and B. Derrida, J. Stat. Phys. **57**, 89 (1989).
[62]N. Evangelou and T. Ziman, J. Phys. C **20**, L235 (1987).
[63]B. Shapiro, Phys. Rev. B **34**, 4394 (1986); Philos. Mag. **56**, 1031 (1987).

[64]A. Cohen, Y. Roth, and B. Shapiro, Phys. Rev. B **38**, 12 125 (1988).

[65]B. Shapiro, Phys. Rev. Lett. **65**, 1510 (1990).

[66]N. I. Akhiezer, *The Classical Moment Problem* (Oliver and Boyd, London, 1965).

[67]B. Derrida, and R. B. Griffiths, Europhys. Lett. **8**, 111 (1989). We used the extension of this scheme to finite temperature, as developed by J. Cook and B. Derrida, J. Stat. Phys. **57**, 89 (1989).

[68]P. W. Anderson, D. J. Thouless, E. Abrahams, and D. S. Fisher, Phys. Rev. B **22**, 3519 (1980).

[69]J. Flores, P. A. Mello, and G. Monsivais, Phys. Rev. B **35**, 2144 (1987).

[70]For a general introduction to the literature on the directed polymer and interface growth problems, see M. Kardar, in *New Trends in Magnetism,* edited by M. D. Coutinho-Filho and S. M. Rezende (World Scientific, Singapore, 1990), p. 277; in *Disorder and Fracture,* edited by J. C. Charmet, S. Roux, and E. Guyon (Plenum, New York, 1990).

[71]D. E. Wolf and J. Kertesz, Europhys. Lett. **4**, 651 (1987).

[72]J. M. Kim and J. M. Kosterlitz, Phys. Rev. Lett. **62**, 2289 (1989).

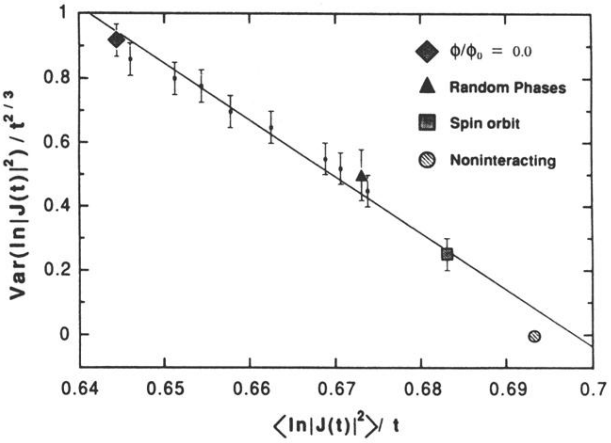

FIG. 19. Complete hierarchy of the exchange attractions between paired paths, reflecting the various Hamiltonian symmetries. Diamond, orthogonal case; triangle, the unitary limit; square, symplectic case; circle, the noninteracting limit corresponding to the IPA, and also to SU(n) with $n \to \infty$. Small squares correspond to finite magnetic fields but no SO.